THE JOURNAL OF PHYSICAL CHEMISTRY C
A JOURNAL OF THE AMERICAN CHEMICAL SOCIETY

pubs.acs.org/JPCC

Article

Cation-Dependent Interfacial Structures and Kinetics for Outer-Sphere Electron-Transfer Reactions

Botao Huang,* Kyaw Hpone Myint, Yanming Wang, Yirui Zhang, Reshma R. Rao, Jame Sun, Sokseiha Muy, Yu Katayama, Juan Corchado Garcia, Dimitrios Fraggedakis, Jeffrey C. Grossman, Martin Z. Bazant, Kang Xu, Adam P. Willard,* and Yang Shao-Horn*

Cite This: *J. Phys. Chem. C* 2021, 125, 4397−4411

Read Online

ACCESS | Metrics & More | Article Recommendations | Supporting Information

ABSTRACT: The kinetics of aqueous outer-sphere electron-transfer (ET) reactions are determined in large part by noncovalent electrostatic interactions that originate from the surrounding electrolyte solution. In this work, we examine the role of spectator cations in modifying the rate of heterogeneous ET for an $[Fe(CN)_6]^{3-}/[Fe(CN)_6]^{4-}$ redox pair. We combine the results of electrochemical measurement, *in situ* surface-enhanced infrared absorption spectroscopy (SEIRAS), classical molecular dynamics simulation, and theoretical modeling to demonstrate how changing the identity of the spectator cation species over a series that includes Li^+, Na^+, K^+, Rb^+ to Cs^+ influences the solvation properties and ET kinetics of the redox species. By analyzing the results in the context of the Marcus−Hush−Chidsey (MHC) theory, we find that the solvent reorganization energy increases systematically as the cationic radius decreases. The trend can be attributed to cation-dependent coordination environments of the redox species, whereby more cations of less charge density such as Cs^+ than Li^+ are present in the redox solvation shell in bulk and at the electrified interface, promoting weaker hydrogen bonds and lowering the effective interfacial static dielectric constant. We discuss the implications of these findings for enabling the tunability of reaction thermodynamics and rates in electrochemical processes.

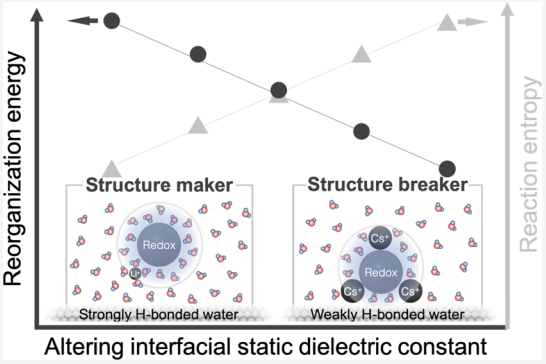

INTRODUCTION

Efficient chemical transformations by electrochemical reactions to generate carbon-free or carbon-neutral energy carriers using solar (and other renewable) energy sources are central to decarbonizing the production of fuels and other commodity chemicals.[1−3] Understanding and controlling the surface electronic structure of catalysts have led to significant advances in the catalytic activity[4] and reaction rates.[4] For example, tuning the *d*-band center relative to the Fermi level[4−7] of metals is shown to govern the binding energy of surface adsorbates and consequently the catalytic activity of numerous reactions including hydrogen evolution[8,9] and oxygen reduction.[5,7] More recently, changing the electrolyte compositions has also been shown to alter the kinetics of electrochemical reactions to exhibit trends such as pH- and cation-dependent kinetics. Specifically, the reaction kinetics of the hydrogen evolution reaction (HER) depend on the pH[10−14] (2 orders of magnitude faster in acid than in base), and inert cations[15,16] (3 orders of magnitude faster and more active with Cs^+ than with Li^+) in the electrolyte, where similar cation-dependent trends have been noted for the oxygen reduction reaction[16−18] and methanol oxidation reaction kinetics.[16] In addition to altering the activity, tuned selectivity in the presence of inactive alkali cations has been reported for CO_2[19,20] and CO[21] reduction reactions due to electrostatic interaction between cations and reaction intermediates.[19−21] Unfortunately, the specific role of electrolytes on the activity[10−12,15−17] and selectivity[19−21] of these multiple-electron electrochemical reactions is not well understood in most cases. Here, we focus on understanding the role of cations in the electrolyte, whose interactions with the redox species are noncovalent, on the kinetics of a simple outer-sphere electron-transfer (ET) reaction.

A large number of experimental and computational studies[22] have examined the role of structure-making or -breaking ions, as described by the structural entropy of ions (<50 J mol^{-1} K^{-1} for structure makers and >50 J mol^{-1} K^{-1} for structure breakers),[22,23] on half-cell reaction entropy[24,25] and cation-[26−33] or anion-[34] dependent kinetics of homogenous[26,30−33] and heterogenous[27−29,34] redox of metal complexes. For example, homogeneous electron-transfer reaction rates (Figure 1a) of metal complexes such as $[Fe(CN)_6]^{3-}/[Fe(CN)_6]^{4-}$

Received: November 21, 2020
Revised: January 31, 2021
Published: February 17, 2021

https://dx.doi.org/10.1021/acs.jpcc.0c10492
J. Phys. Chem. C 2021, 125, 4397−4411

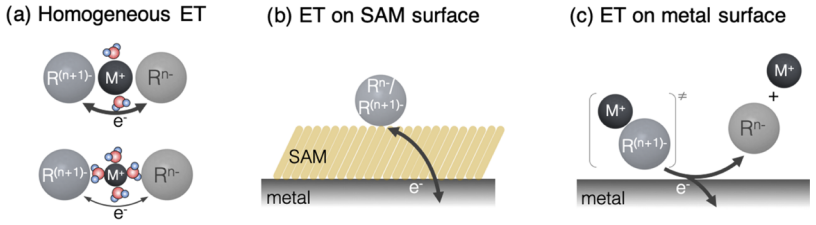

Figure 1. Schematic of electron-transfer mechanisms in homogeneous and heterogeneous processes. (a) In a homogeneous electron-transfer reaction, spectator cations in the electrolyte have been proposed to bridge two redox anions, where Cs^+ is partially dehydrated (hydration energy at -283 kJ mol^{-1}) and facilitates ion pairing and electron transfer, while Li^+ is difficult to deaquate (hydration energy at -531 kJ mol^{-1}), and thus the larger electron-transfer barrier. (b) In heterogeneous electron transfer at the metal surface coated by a self-assembled monolayer, where the redox molecules are held by the film at a fixed distance from the electrode surface. (c) In heterogeneous electron transfer at the metal surface, an activated complex associated with spectator cations of the supporting electrolyte and redox anions could be formed by ion association/pairing, which could change the electroaffinity and ionization energy of redox species, and thus the altered kinetics.

measured by nuclear magnetic resonance (NMR) are strongly influenced by the nature of added cations ($Li^+ < Na^+ < K^+ < Rb^+ < Cs^+$).[26,30,31,33] This trend can be attributed to cation catalysis involving the formation of a bridge between two redox anions by a cation, where the less hydrated cations approach anions closer and lead to faster reaction rates.[26] Smaller cations with a higher charge density (*e.g.*, Li^+ and Na^+) tend to interact more strongly with water molecules than their larger counterparts (*e.g.*, Cs^+ and Rb^+).[22,23] In addition, the electron-transfer kinetics of metal complexes[35−38] tethered to the terminal of a self-assembled monolayer (SAM) of an alkane thiol (Figure 1b) have shown that the reorganization energy increases and the rate constant of electron transfer decreases with increasing the SAM thickness of ferrocene/ferrocenium ($Fe(C_5H_5)_2^{+/0}$),[35−37] $Ru^{2+/3+}$,[35,38] and 4-[*N*,*N*-di(*p*-tolyl)-amino]benzylphosphonic acid ($TPA^{+/0}$).[38]

The electron-transfer reaction rate of $[Fe(CN)_6]^{3-}/[Fe(CN)_6]^{4-}$ redox (Figure 1c on the metal surface) is cation-dependent ($Li^+ < Na^+ < K^+ < Rb^+ \sim Cs^+$),[27−29] and the reaction rate of the NpO_2^{2+}/NpO_2^+ redox center is anion-dependent ($ClO_4^- \sim NO_3^- > Cl^- > SO_4^{2-} >$ acetate$^-$).[34] These trends have been attributed to the association of spectator ions with redox centers, which could tune the energetics of activated complexes in their transition states,[27−29,34] leading to faster rates for systems with more weakly hydrated cations. However, the influence of these spectator ions on the solvation properties of the environment of the electrified interface is yet to be fully understood. In addition, while spectator cations and anions have been used extensively to alter the reaction rates of homogenous and heterogeneous reactions for the redox of metal complexes, their role on the reorganization energy has been rarely reported even though the reaction rate scales inversely with the reorganization energy in the Marcus theory[39,40] for homogeneous electron-transfer reactions or the Marcus−Hush−Chidsey (MHC) formalism[39,41−43] for heterogeneous (faradic) reactions at electrodes. The solvent reorganization energy of heterogeneous electron-transfer reactions has been shown to decrease as the redox centers move closer to the electrode surface,[44,45] which is in agreement with models based on the dielectric continuum theory, predicting a decrease in the electron-transfer reorganization energy with decreasing distance between the redox center and the electrode,[46,47] as well as classical molecular dynamics (MD) simulation.[48] Moreover, while previous Raman and Fourier transform infrared (FTIR) spectroscopy studies have shown that the solvation structure of the redox species in bulk can be altered by spectator cations,[24] much remains to be understood about how they influence the solvation environment at the electrified interface. Understanding this influence is critical to understanding spectator-ion-dependent static dielectric constants underpinning potential changes in the reorganization energy.

In this study, we explore a series of spectator cations that are redox-inactive yet perturb both the solvation environment of $[Fe(CN)_6]^{3-}/[Fe(CN)_6]^{4-}$ at the electrified interface and the redox kinetics. The redox species-spectator ion radial distribution function (RDF), calculated from classical MD simulations, shows a decreased number of water molecules and increased number of cations in the solvation environments of $[Fe(CN)_6]^{3-}/[Fe(CN)_6]^{4-}$ in the order from Li^+ to Cs^+. The kinetic currents of equimolar $[Fe(CN)_6]^{3-}/[Fe(CN)_6]^{4-}$ in an aqueous solution containing chloride salts of Li^+, Na^+, K^+, Rb^+, and Cs^+ have been extracted using a polycrystalline Au rotating disc electrode (RDE). The exchange current density j_0 increases with greater structure-breaking ions on the order of $Li^+ < Na^+ < K^+ < Rb^+ < Cs^+$, which is correlated with a reduction in the reorganization energy λ *via* the MHC theory,[41−43] decreasing from 0.59 to 0.23 eV in the order of $Li^+ > Na^+ > K^+ > Rb^+ > Cs^+$. The increased exchange current density and reduced reorganization energy found for $[Fe(CN)_6]^{3-}/[Fe(CN)_6]^{4-}$ can be attributed to having an increased number of cations and decreased number of water molecules at the electrified interface. We support this claim based on *in situ* surface-enhanced infrared absorption spectroscopy (SEIRAS) measurements, which reveal an increasing fraction of weakly H-bonded water molecules (in the order of $Li^+ < K^+ < Cs^+$) and a decreasing fraction of strongly H-bonded water molecules (in the order of $Li^+ > K^+ > Cs^+$) from Li^+ to Cs^+. Invoking the Born model, we hypothesize that the cation-dependent properties of the interfacial solvation environment also extend to the static dielectric constant, which we infer to be much lower than that of the bulk and decreasing from Li^+ to Cs^+. In addition, this argument is in agreement with the predicted reaction entropy using the Born model and the experimental results. This work thus advances a molecular picture of how spectator cations alter the interfacial water structure and the solvation structure of negatively charged redox molecules, which consequently alter the exchange current densities and the reorganization energy of electron-transfer kinetics.

METHODS

Classical Molecular Dynamics (MD) Calculations. Classical molecular dynamics (MD) simulations were carried

https://dx.doi.org/10.1021/acs.jpcc.0c10492
J. Phys. Chem. C 2021, 125, 4397−4411

out on two types of systems. The first system, used for bulk-phase Madelung potential energy distribution analysis (Appendix S1), contained a representation of the bulk aqueous electrolyte in a cubic simulation cell periodically replicated in all directions with 10 738 water molecules, modeled using the SPC/E force field[49] and 119 alkali ions (Li^+, Na^+, K^+, Rb^+, Cs^+) with an equal number of Cl^- as their counterions, roughly corresponding to a 0.6 M (~90 water molecules per ion) concentration of cations. For alkali ions, the Lennard-Jones (LJ) parameters from ref 50 were adopted along with the scaled-ionic-charge model to account for electronic polarization effects in a classical nonpolarizable force field.[51−53] The second system, used to compute the solvation structure and energetics of $[Fe(CN)_6]^{3-}/[Fe(CN)_6]^{4-}$, contained 7336 water molecules, 80 alkali ions (~0.6 M), 80 Cl^- anions, and 8 $[Fe(CN)_6]^{3-}/[Fe(CN)_6]^{4-}$ anions each (~60 mM), where $[Fe(CN)_6]^{3-}/[Fe(CN)_6]^{4-}$ anions' LJ parameters were adopted from the PCFF+ force field,[54,55] as implemented in the commercialized simulation environment MedeA,[56] with the set of bonding parameters that well-reproduced the molecule structures in water.[57] Lorentz−Berthelot mixing rules were used to derive mixed Lennard-Jones parameters. All of the parameters used are summarized in Table S1.

For all of the systems, simulations were performed in LAMMPS using periodic boundary conditions. A particle-mesh Ewald algorithm with a real-space cutoff value of 9 Å was used to calculate long-range electrostatic interactions. The temperature and pressure during the equilibration periods were maintained by a Nose−Hoover thermostat and a barostat, respectively, at 300 K and 1 atm. Furthermore, the bonds and angles of SPC/E water were constrained by the Shake algorithm.[58] The system was initially equilibrated in the NPT ensemble with a time step of 2 fs for a total equilibration time of 0.1 ns to achieve an equilibrium density before equilibrating again in the NVT ensemble for another 0.1 ns. A final production run of 1 ns was then performed in the NVE ensemble to collect good statistic.[49]

The interaction energy is defined as the total interaction between the $[Fe(CN)_6]^{3-}/[Fe(CN)_6]^{4-}$ anions and water molecules in the system normalized by the number of $[Fe(CN)_6]^{3-}/[Fe(CN)_6]^{4-}$ anions, which can be described by the following equation

$$E = \frac{\sum_{i=1:N}\sum_{j=1:M} U_{ij}}{N} \tag{1}$$

where N is the number of $[Fe(CN)_6]^{3-}/[Fe(CN)_6]^{4-}$ molecules, M is the number of water molecules, and U_{ij} is the interaction energy between each ij molecule pair (including both the van der Waals and the Coulombic contribution). The values of the interaction energy are the averaged values for a time span of 3 ns of MD simulations with a saving frequency of 0.2 ps. The error bar is the standard deviation of these data (15 000 data points).

Electrochemical Measurements and Electrolyte Preparation. All electrochemical measurements were conducted with a Biologic SP-300 potentiostat in an isothermal three-electrode electrochemical system[24] under an Ar atmosphere, where the temperature was controlled by a thermal bath circulator (Thermo Neslab RTE 7). The working electrode was a Pt or an Au rotating disk electrode (RDE) (Pine Instrument). Potentials were referenced to a mercury sulfate ($Hg/HgSO_4$) reference electrode (MSE). The effect of cations in the supporting electrolyte on the kinetics of $[Fe(CN)_6]^{3-}/[Fe(CN)_6]^{4-}$ redox was examined by cyclic voltammetry (CV) at a scan rate of 10 mV s^{-1} at 293 K, where the current density was obtained based on the geometric surface area of RDE (0.196 cm^2). In these electrochemical measurements, electrolytes consisted of 2 mM equimolar $[Fe(CN)_6]^{3-}/[Fe(CN)_6]^{4-}$ and 0.06, 0.2, 0.4, and 0.6 M chloride salts of Li^+, Na^+, K^+, Rb^+, Cs^+, or tetrabutylammonium$^+$ (TBA^+). For temperature-dependent measurements, the temperature of the electrochemical cell was increased from 293 to 323 K in increments of 10 K. The $[Fe(CN)_6]^{3-}/[Fe(CN)_6]^{4-}$ solution was prepared from deionized water (Millipore, >18.2 MΩ cm), potassium hexacyanoferrate(III) (>99%, Alfa Aesar), and potassium hexacyanoferrate(II) trihydrate (99.5%, Sigma-Aldrich). For cation-dependent measurements, tetrabutylammonium chloride (TBACl, >98%, Sigma-Aldrich), lithium chloride (>99.98%, Sigma-Aldrich), sodium chloride (99.99%, Sigma-Aldrich), potassium chloride (99.995%, Sigma-Aldrich), rubidium chloride (99.8%, Sigma-Aldrich), and cesium chloride (99.9%, Sigma-Aldrich) were used.

To extract the kinetic current density, we performed cyclic voltammetry (CV) with RDE at rotation rates of 400, 900, 1600, and 2500 rpm, as shown in Figure S1. Kinetic current density can be extracted from rotation-rate-dependent CV using the traditional Koutechy−Levich equation (slow kinetic model)[59]

$$\frac{1}{j} = \frac{1}{j_k'} + \frac{1}{j_L} = \frac{1}{j_k'} + \frac{1}{0.62nFA'D_O^{2/3}\omega^{1/2}\nu^{-1/6}C_O^*} \tag{2}$$

where j denotes the measured current density; j_k' is the kinetic current density from the slow kinetic model; j_L is the limiting current density; n is the number of electrons transferred during the reaction; F is the Faraday constant; A' is the surface of the electrode; D_O and C_O^* are the diffusion coefficient and bulk concentration of the oxidant, respectively; ν is the cinematic viscosity of the electrolyte; and ω is the rotation rate. The model assumes that (1) the redox process is a reversible and first-order reaction; and (2) the electron-transfer rate is slow (*e.g.*, $j_k'/j_L < 0.1$) and governed by kinetics rather than mass transport, where the current is described by $j = FA'k_f(E)C_O(y = 0)$, where y is the distance from the electrode surface. However, for electrochemical reactions in moderate and fast kinetic regions (*e.g.*, $0.1 < j_k'/j_L < 1$), the current could be limited by mass transport, $j = nfA'D_O[C_O^* - C_O(y = 0)]/\delta_O$, with δ_O denoting the diffusion-layer thickness of the oxidant at an electrode. In this regime, the fast kinetic model[59] can be more accurate for the Koutechy−Levich analysis

$$\frac{1}{j} = \frac{1}{FA'(k_fC_O^* - k_bC_R^*)} + \frac{D_O^{-2/3}k_f + D_R^{-2/3}k_b}{0.62\nu^{-1/6}\omega^{1/2}} = \frac{1}{j_k} + \frac{D_O^{-2/3}k_f + D_R^{-2/3}k_b}{0.62\nu^{-1/6}\omega^{1/2}} \tag{3}$$

where D_R denotes the diffusion coefficient of the reductant and k_f and k_b are the rate constants of forward and backward reactions, respectively. Instead of the constant slope of the plot $1/j$ vs $\omega^{-0.5}$ in the traditional Koutechy−Levich equation (slow kinetic model, eq 2), the fast kinetic model (eq 3) proposes varied slopes (Figure S2) due to the overpotential-dependent k_f and k_b. The electron-transfer process of 2 mM $[Fe(CN)_6]^{3-}/[Fe(CN)_6]^{4-}$ in the aqueous electrolyte of 0.6 M chloride salts of Li^+, Na^+, K^+, Rb^+, and Cs^+ is reversible (Figure

https://dx.doi.org/10.1021/acs.jpcc.0c10492
J. Phys. Chem. C 2021, 125, 4397−4411

S3a). The slow kinetic region for $j_k'/j_L < 0.1$ was located at an overpotential range within a few millivolts for both oxidation and reduction, which is too narrow to explore kinetic parameters using electron-transfer theories. Moderate and fast kinetic regions for $0.1 < j_k'/j_L < 1$ were located at overpotential ranges up to 30−70 mV (*e.g.*, 30 mV for K^+, Rb^+, and Cs^+; 50 mV for Li^+ and Na^+; 70 mV for TBA^+; see Figure S4) for the Au electrode, where the fast kinetic model could be more suitable for the extraction of kinetic current.

To extract kinetic parameters, including reorganization energy, from the kinetic current density, the Butler−Volmer equation and the Marcus−Hush−Chidsey (MHC) formalism[41,42] have been employed. The widely used Butler−Volmer equation is an empirical relationship, which can be motivated by assuming that the electrostatic energy of the reaction transition state of the reaction is an average of the reduced and oxidized states, weighted by the charge-transfer coefficient. In contrast, the microscopic MHC formalism accounts for the quantum mechanical nature of electron transfer and considers the solvent reorganization energy of the solvation shell and the electron energy levels in the metal electrode, which can be more accurate and predictive for reactions at liquid−solid interfaces.

$$j_{red/ox}^{MHC}(\eta) = A\int_{-\infty}^{\infty} \exp\left(-\frac{(x - \lambda \pm e\eta)^2}{4\lambda k_B T}\right) \frac{dx}{1 + \exp(x/k_B T)} \quad (4)$$

$$A = \frac{2\pi H_{AB}^2}{h(4\pi\lambda k_B T)^{1/2}} \quad (5)$$

where λ is the reorganization energy, k_B is the Boltzmann constant, T is temperature, η is the overpotential, and A is the pre-exponential factor,[39,40] accounting for the electronic coupling strength, where h is the Plank constant and H_{AB} is the electronic coupling energy. The electronic density of states (DOS) of the electrode, x, accounts for the Fermi statistic of electron energies distributed around the electrode potential. The first term in the integrand is the classical Marcus rate for the transfer of an electron of energy x relative to the Fermi level, and the second factor is the Fermi−Dirac distribution assuming a slowly varying DOS, which to first approximation can be considered uniform. The corresponding exchange current density can be calculated as follows[41]

$$j_0 = \frac{2\pi H_{AB}^2}{h\sqrt{4\pi\lambda k_B T}} \frac{\sqrt{\pi\lambda}}{2} \operatorname{erfc}\left(\frac{\lambda - \sqrt{1 + \sqrt{\lambda}}}{2\sqrt{\lambda}}\right) \quad (6)$$

The MHC formalism also includes the standard free energy of activation, which consists of the inner-sphere and outer-sphere contributions arising from the structural reorganization of the reactants and the surrounding solvent. The solvation free energy of reactants is largely based on the Born model, assuming that the solvent is a dielectric continuum and each reactant is treated as a sphere, having the first solvation layer dielectrically saturated.

The activation energy of the $[Fe(CN)_6]^{3-}/[Fe(CN)_6]^{4-}$ redox reaction has been estimated from temperature-dependent exchange current density *via* the Arrhenius equation[27]

$$j_0 = A \exp\left(-\frac{E_a - T\Delta S^{\neq}}{RT}\right) \quad (7)$$

and our analysis will compare this approach with the MHC formalism (eqs 4−6).

X-ray Absorption Spectroscopy (XAS). X-ray absorption spectroscopy measurements at the iron K-edge (7112 eV) were performed at the inner-shell spectroscopy (ISS) 8-ID at the National Synchrotron Light Source II at Brookhaven National Laboratory (BNL). The sample holders (2 × 2 cm^2 polyethylene resealable bags) were filled with 200 μL of electrolyte and mounted at an angle of roughly 45° with the respect to both the incident beam and the detectors. The irradiated spot size on the sample was about 25 μm in diameter. All measurements were made at room temperature in the fluorescence mode. All samples were measured with a Fe metal foil reference simultaneously for correct energy alignment of individual spectra during data analysis. Data processing (spectra alignment, averaging, and normalization) was done using Athena. Normalized spectra were fitted utilizing Artemis with theoretical structural models created with FEFF6. A higher concentration than that used in electrochemical measurements, 0.2 M ($K_3Fe(CN)_6$ or $K_4Fe(CN)_6$), was used in the XAS measurements to obtain reliable XAS signals. Chloride salt (2 M) of CsCl, RbCl, KCl, NaCl, LiCl, or TBACl was added to have a reasonable cation/redox ratio, allowing for the observation of the appropriate cation effect.

***In Situ* Surface-Enhanced Infrared Absorption Spectroscopy (SEIRAS).** Pt or Au was deposited on a hemispherical Si prism (radius 22 mm, Pier Optics). The prism was mounted on a spectro-electrochemical three-electrode cell with a Ag/AgCl reference electrode and a platinum-wire counter electrode. The SEIRAS spectra were obtained with a Fourier transform infrared (FTIR) Vertex 70 (Bruker) spectrometer equipped with an mercury−cadmium−telluride (MCT) detector. The optical path was fully replaced with N_2 gas. The SEIRAS spectra were obtained with 4 cm^{-1} resolution at 7.5 kHz scan velocity in the 500−4000 cm^{-1} spectral range; 128 scans were averaged. The SEIRAS spectra were recorded using a single-reflection attenuated total reflection (ATR) accessory (Pike Vee-Max II, Pike Technologies) with a Si prism at an incident angle of 68°. Further details of *in situ* SEIRAS can be found elsewhere.[60] For *in situ* SEIRAS measurements, electrolytes consisted of 2 mM $[Fe(CN)_6]^{4-}$ or $[Fe(CN)_6]^{3-}$ and 0.6 M chloride salts of Li^+, K^+, or Cs^+. To further amplify the cation effect, the measurements were repeated in electrolytes at a higher concentration, consisting of 0.1 M $[Fe(CN)_6]^{4-}$ or $[Fe(CN)_6]^{3-}$ and 2 M chloride salts. After deoxygenation of the electrolyte solution, obtained by purging Ar, the prism surface was cleaned by cycling the potential between 0.6 and 1.2 V_{RHE}. The equilibrium potential is ~0.9 V_{RHE} for electrolytes containing 0.1 M $[Fe(CN)_6]^{4-}$ or $[Fe(CN)_6]^{3-}$ and 2 M chloride salts. For the oxidation of $[Fe(CN)_6]^{4-}$, the reference spectrum I_0 was measured at 0.5 V_{RHE} in the electrolytes containing $[Fe(CN)_6]^{4-}$ and chloride salt. SEIRAS spectra were collected at 0.7, 0.9, and 1.1 V_{RHE} at room temperature. During the reduction of $[Fe(CN)_6]^{3-}$, the reference spectrum I_0 was measured at 1.2 V_{RHE} in the electrolytes containing $[Fe(CN)_6]^{3-}$ and chloride salt. SEIRAS spectra were collected at 1.1, 0.9, and 0.7 V_{SHE} at room temperature. All spectra are shown in absorbance units defined

https://dx.doi.org/10.1021/acs.jpcc.0c10492
J. Phys. Chem. C 2021, 125, 4397−4411

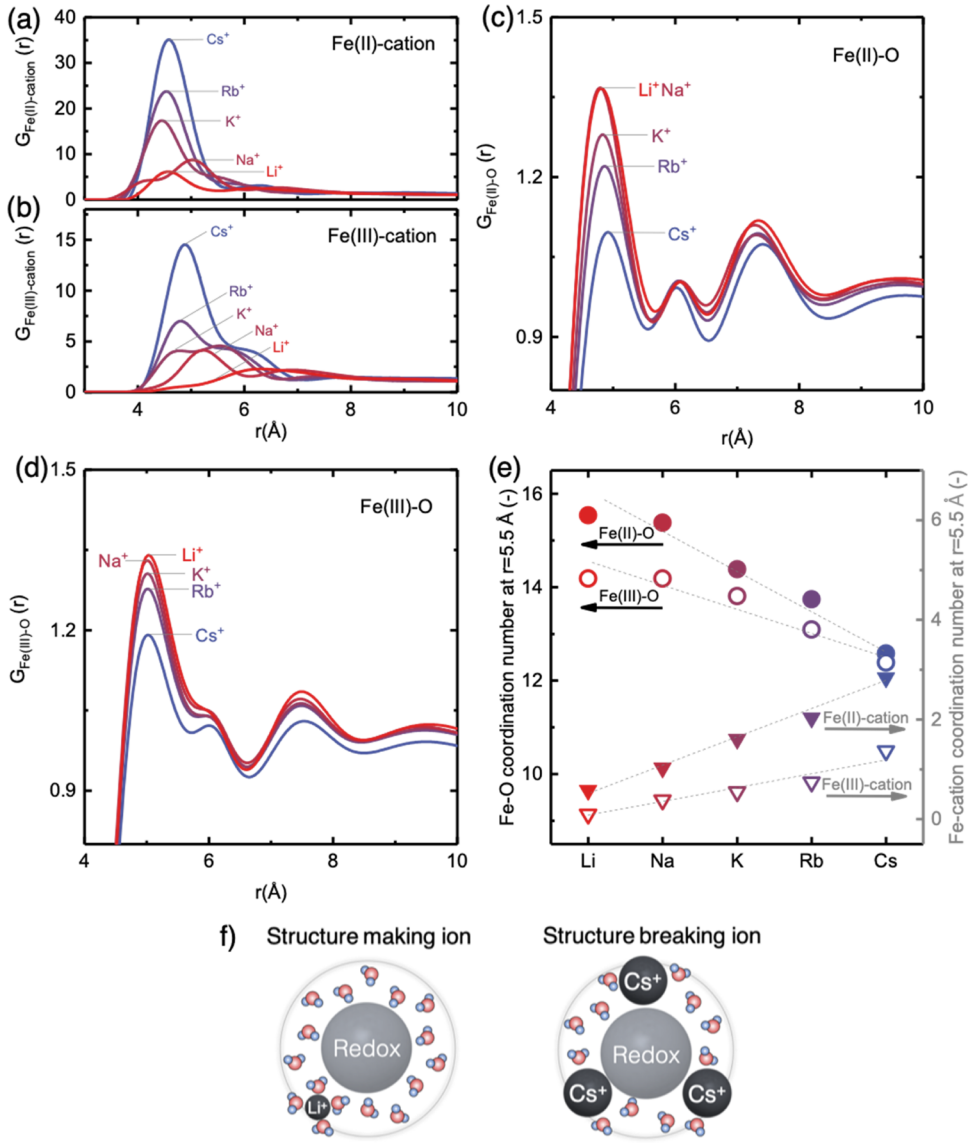

Figure 2. Changes in the water and cation occupancy within the first solvation shell of the $[Fe(CN)_6]^{3-}/[Fe(CN)_6]^{4-}$ redox center calculated using classical MD simulation. Systems contain 7336 water molecules, 80 cations, 80 Cl^- ions, and 8 molecules of $[Fe(CN)_6]^{4-}$ and $[Fe(CN)_6]^{3-}$ each in the presence of different chloride salts of Li^+, Na^+, K^+, Rb^+, and Cs^+ in classical MD simulations, corresponding to 60 mM $[Fe(CN)_6]^{3-}/[Fe(CN)_6]^{4-}$ and 0.6 M chloride salts in water. Fe-cation radial distribution function (RDF) for (a) $[Fe(CN)_6]^{4-}$ and (b) $[Fe(CN)_6]^{3-}$. Fe−O RDF for (c) $[Fe(CN)_6]^{4-}$ and (d) $[Fe(CN)_6]^{3-}$. (e) Fe−O and Fe-cation coordination number at the outer boundary of the first solvation shell (r = 5.5 Å) along the sequence of different cations, revealing that the decrease in water molecules is compensated for by an increase in cations. (f) Schematic showing the altered redox $[Fe(CN)_6]^{4-}$ solvation shell by 1 Li^+ with 16 water molecules and 3 Cs^+ with 12 water molecules. For the coordination number of Fe-cation and Fe−O as well as N−H RDF and coordination number of $[Fe(CN)_6]^{4-}$ and $[Fe(CN)_6]^{3-}$, please refer to Figure S6.

as $\log(I_0/I)$, where I_0 and I represent the spectra at the reference and sample potentials, respectively.

For *ex situ* ATR/FTIR measurements of bulk electrolytes, the spectra were acquired in the ATR mode using a Si prism (Pier Optics) without surface deposition at an incident angle of 70°. Spectral settings were the same as *in situ* SEIRAS measurements.

RESULTS AND DISCUSSION

Cation-Dependent Solvation Structures of Redox Anions and Cations from Molecular Dynamics Simulations. The results from the MD simulation show that the local solvation environment of redox anions is strongly cation-dependent. Analysis of the Fe-cation radial distribution functions (RDFs) reveals increasing first peak intensity in the order of $Li^+ < Na^+ < K^+ < Rb^+ < Cs^+$, as illustrated in Figure 2a,b. In addition, the first peak in the RDF was found to be narrower for $[Fe(CN)_6]^{4-}$ than for $[Fe(CN)_6]^{3-}$, suggesting that the more highly charged anion binds neighboring cations more tightly. This difference can be attributed to stronger Coulombic interactions associated with the higher charge of $[Fe(CN)_6]^{4-}$, in agreement with previous works.[25,57] On the other hand, RDFs of Fe−O for $[Fe(CN)_6]^{4-}$ (Figure 2c) and $[Fe(CN)_6]^{3-}$ (Figure 2d) had broad distributions centered at ~5.0 Å for all of the cations, with decreasing peak intensities in the order of $Li^+ > Na^+ > K^+ > Rb^+ > Cs^+$, as illustrated in Figure 2c,d. By integrating over the first peak, we find that the coordination number of water molecules in the solvation

https://dx.doi.org/10.1021/acs.jpcc.0c10492
J. Phys. Chem. C 2021, 125, 4397−4411

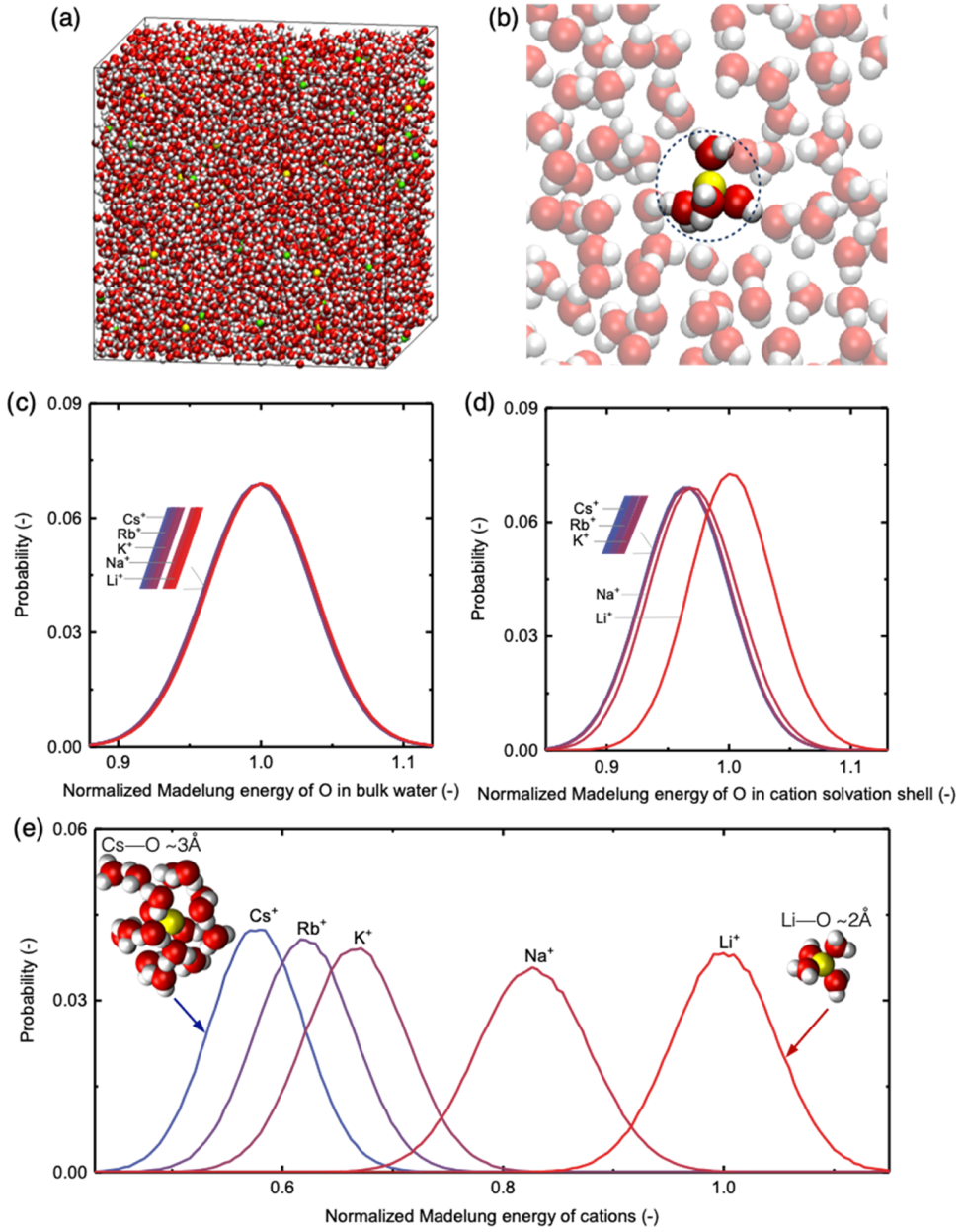

Figure 3. Electrostatic potential distribution analysis of systems containing 10 738 water molecules, 109 cations, and 109 Cl^- ions in classical MD simulation, corresponding to 0.6 M chloride salts in water. (a) Image of the unit cell of the simulation; (b) image highlighting a Li^+ ion surrounded by four water molecules in its first solvation shell; (c) Madelung potential energy distribution of the oxygen atoms in bulk water molecules; (d) Madelung potential energy distribution of the oxygen atoms of water molecules in the solvation shell of cations; and (e) Madelung potential energy distribution of cations. The Madelung potential energy was normalized to the Li^+ case.

sphere decreases from approximately 16 to 12 for $[Fe(CN)_6]^{4-}$ as the cation is changed from Li^+ to Cs^+ (and from approximately 14 to 12 for $[Fe(CN)_6]^{3-}$), respectively. These results are plotted in Figure 2e. This trend is in agreement with the decreasing interaction energy, E (see eq 1), between $[Fe(CN)_6]^{3-}/[Fe(CN)_6]^{4-}$ and water in the order of $Li^+ > Na^+ > K^+ > Rb^+ > Cs^+$ (more information on the interaction energy is available in Figure S5). The reduced coordination of water molecules from $Li^+ > Na^+ > K^+ > Rb^+ > Cs^+$ was accompanied by the increased coordination with cations (Figure 2e), indicating that cations are displacing water molecules within the first solvation shell of the redox species, as illustrated in Figure 2f.

To better understand the influence of different cations on the electrostatic fluctuations of the bulk electrolyte solution, we analyzed the electrostatic potential fluctuations felt by various species in solution. We quantify these fluctuations in terms of the probability distribution of the Madelung potential (Appendix S1) evaluated for cations and the oxygen of water molecules inside and outside of the cationic solvation shell. The fluctuations in this potential drive Marcus-like outer-sphere electron-transfer reactions. The width of the associated probability distribution in particular can be related to the reorganization energy.[48]

Figure 3a shows the structure of the simulation cell containing 0.6 M LiCl in water, and Figure 3b highlights the aqueous solvation environment of Li^+. The electrostatic

https://dx.doi.org/10.1021/acs.jpcc.0c10492
J. Phys. Chem. C 2021, 125, 4397−4411

potential distributions for water oxygen in the bulk of the electrolyte were found to exhibit negligible dependence on the identity of the cation species, as illustrated in Figure 3c. This observation implies an expectation that the long-range contribution of electrolyte fluctuations to the bulk water structure should be cation-independent. Hence, we focus more specifically on the region around the cations. Figure 3d contains a plot of the Madelung potential distribution for the oxygen of water molecules within the first solvation shell of a cation. We observe that with the exception of Li^+, the distributions are nearly identical, suggesting that even local electrostatic fluctuations are not strongly affected by the cations. For Li^+, strong water coordination shifts the mean but reduces the variance only slightly. Notably, the widths of these distributions do not exhibit the systematic changes that would be required to account for observations of cation-dependent ET rates in homogeneous reactions reported previously.[26,30,31,33] We thus conclude that these observations arise through the changes in redox solvating structures due to noncovalent interactions associated with redox centers, spectator cations, and water molecules.

This conclusion is further supported by calculations of the potential distributions at the positions of the cations themselves. As Figure 3e illustrates, these distributions vary systematically in their mean and variance as the identity of the cation is changed, with the mean and variance increasing as $Cs^+ < Rb^+ < K^+ < Na^+ \ll Li^+$ (Figure 3e). More detailed information about these calculations is presented in the Supporting Information (Figure S7). Below, we examine the influence of cation-dependent solvation environments of redox anions and cations in the electrolyte on the electron-transfer kinetics of the $[Fe(CN)_6]^{3-}/[Fe(CN)_6]^{4-}$ redox couple.

Cation-Dependent Exchange Current Densities of the $[Fe(CN)_6]^{3-}/[Fe(CN)_6]^{4-}$ Redox Couple. RDE measurements show that the electron-transfer kinetics of $[Fe(CN)_6]^{3-}/[Fe(CN)_6]^{4-}$ are strongly dependent on the nature of cations in the electrolyte (Figures 4 and S8), increasing in the sequence of tetrabutylammonium$^+$ (TBA^+) < Li^+ < Na^+ < K^+ < Rb^+ < Cs^+. Cyclic voltammogram of 2 mM equimolar $[Fe(CN)_6]^{3-}/[Fe(CN)_6]^{4-}$ dissolved in Ar-saturated 0.6 M LiCl and KCl collected from an Au RDE revealed a well-defined kinetics-limiting regime (overpotential of ~±0.03 V) and linear increments of transport-limiting currents with increasing rotation speeds from 400, 900, 1600 to 2500 rpm at 293 K, as shown in Figure 4a,b, respectively. Kinetic currents of the $[Fe(CN)_6]^{3-}/[Fe(CN)_6]^{4-}$ redox couple were obtained by removing the influence of transport from rotation-dependent currents using a method typically used for fast electron-transfer reactions[59] (eq 3 and Figure S2 for the Koutecky–Levich plot). The kinetic current density normalized by the geometric surface area (0.196 cm^2) of Au RDE is shown in Figure 4c, from which the exchange current density, j_0, was extracted. Comparable exchange current densities were obtained from the Butler–Volmer (triangles in Figure 4d) and MHC analyses[41−43] (circles in Figure 4d), which were found to increase by 2 orders of magnitude in the sequence of tetrabutylammonium$^+$ (TBA^+) < Li^+ < Na^+ < K^+ < Rb^+ < Cs^+, from 0.2 for Li^+ to 22.6 mA cm^{-2} for Cs^+. Similar cation-dependent kinetics have been reported for $[Fe(CN)_6]^{3-}/[Fe(CN)_6]^{4-}$ by electrochemical impedance spectroscopy on Au,[29] a current impulse method on Au,[27] and a microelectrode study on Pt[61] and for the reaction constants for self-exchange reactions of $[Os(CN)_6]^{3-}/[Os(CN)_6]^{4-}$,[26,33] $[Mo(CN)_8]^{3-}/[Mo(CN)8]^{4-}$,[26] and $[W(CN)_8]^{3-}/[W(CN)8]^{4-}$[26] measured by NMR.[26,33]

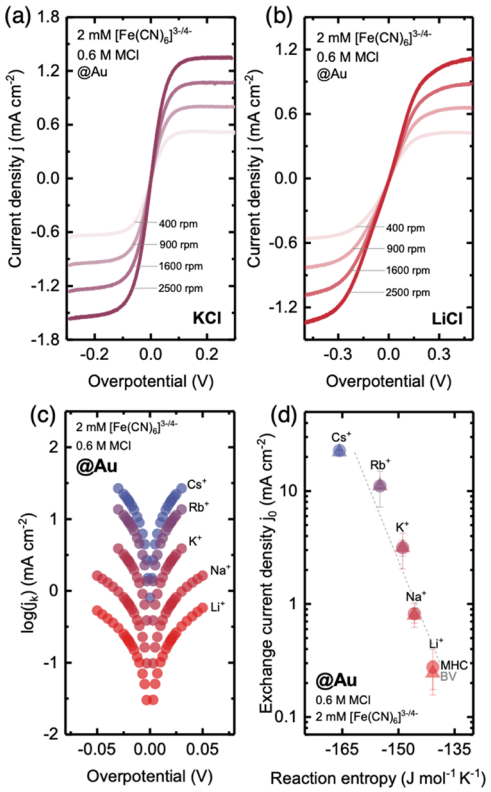

Figure 4. Cation-dependent kinetics of 2 mM equimolar $[Fe(CN)_6]^{3-}/[Fe(CN)_6]^{4-}$ in aqueous electrolyte electrodes. Cyclic voltammograms measured in an Ar-saturated aqueous solution of 0.6 M (a) KCl and (b) LiCl on the Au RDE electrode at 10 mV s^{-1} and 400, 900, 1600, and 2500 rpm at 293 K. (c) Kinetic current density j_k measured on Au and extracted by the fast kinetic model of Koutecky–Levich analysis[59] (eq 3). (d) Exchange current density j_0 measured on Au fitted by the Butler–Volmer and MHC formalisms[41] for the fast kinetic model. The values of reaction entropy were taken from ref 24. Error bars were obtained from the standard deviation of three independent measurements.

The cation-dependent trend in the exchange current density remained when the concentration of cations was decreased from 0.6 to 0.06 M (Figure S9). The exchange current density of 2 mM $[Fe(CN)_6]^{3-}/[Fe(CN)_6]^{4-}$ decreased linearly on lowering the concentration of cations in the supporting electrolyte (Figure S9a). For example, the exchange current density decreased from 0.24 to 0.01 mA cm^{-2} for Li^+ and from 3.15 to 0.2 mA cm^{-2} for K^+ when the concentration of MCl was changed from 0.6 to 0.06 M. The first reaction order on the cation concentration (Figure S9a) is in agreement with the previously reported reaction order found for the exchange current density of $[Fe(CN)_6]^{3-}/[Fe(CN)_6]^{4-}$ redox (KCl)[27] and for the rate constants of self-exchange reactions of $[Os(CN)_6]^{3-}/[Os(CN)_6]^{4-}$,[26,33] $[Mo(CN)_8]^{3-}/[Mo(CN)_8]^{4-}$,[26] and $[W(CN)_8]^{3-}/[W(CN)_8]^{4-}$[26] in the electrolytes of chloride salts of Li^+, Na^+, K^+, Rb^+, and Cs^+ from NMR measurements.[26,33] The exchange current density of 2 mM equimolar $[Fe(CN)_6]^{3-}/[Fe(CN)_6]^{4-}$ redox in the presence of cations in the electrolyte such as K^+ translates to a heterogeneous reaction rate constant k^0_{hetero} of 0.016 cm s^{-1}, which is in agreement with those from previous RDE studies reported by Kůta et al. (0.02 cm s^{-1}),[28] Angell et al. (0.02 cm

https://dx.doi.org/10.1021/acs.jpcc.0c10492
J. Phys. Chem. C 2021, 125, 4397−4411

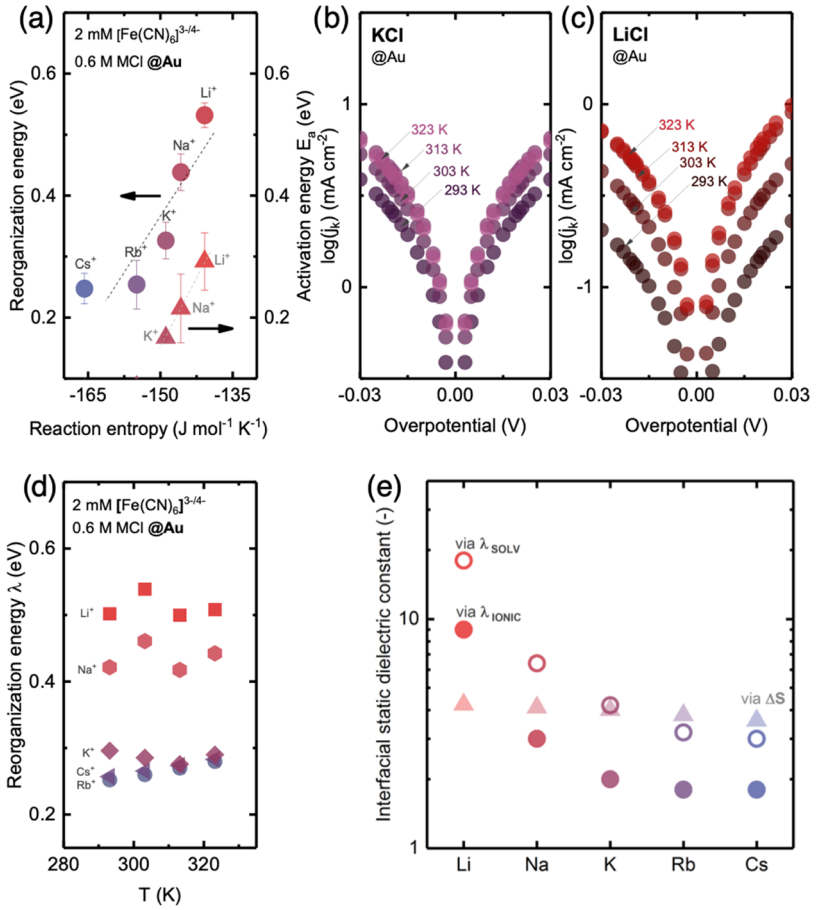

Figure 5. Temperature-dependent kinetics of 2 mM equimolar $[Fe(CN)_6]^{3-}/[Fe(CN)_6]^{4-}$ in an Ar-saturated aqueous solution containing 0.6 M chloride salts measured on Au. (a) Reorganization energy (solid circle) and activation energy E_a (open triangle) from the Arrhenius expression of exchange current densities of $[Fe(CN)_6]^{3-}/[Fe(CN_6)]^{4-}$ against the experimental reaction entropy of $[Fe(CN)_6]^{3-}/[Fe(CN)_6]^{4-}$ redox taken from a previous work.[24] Error bars were obtained from the standard deviation of three independent measurements. Temperature-dependent kinetic current density at 293−323 K in 0.6 M (b) KCl and (c) LiCl. (d) Reorganization energy of $[Fe(CN)_6]^{3-}/[Fe(CN_6)]^{4-}$ as a function of temperature in electrolytes with different cations. The temperature-dependent measurements of $[Fe(CN)_6]^{3-}/[Fe(CN)_6]^{4-}$ redox on Au in the presence of Cs^+ and Rb^+ (Figure S10a,b) as well as kinetic measurements on Pt were found to have large experimental uncertainty (Figures S11 and S12), which can be attributed to either significant mass transport limitation due to fast kinetics of $[Fe(CN)_6]^{3-}/[Fe(CN)_6]^{4-}$ (Figure S13 for the ratio of kinetic current density over limiting current density) or the degradation of $[Fe(CN)_6]^{3-}/[Fe(CN)_6]^{4-}$ on the electrode surface reported previously.[87,88] (e) Interfacial static dielectric constant extracted *via* reorganization energy without (λ_{SOLV}, eq 8) and with (λ_{IONIC}, eq 9) ionic environment effects and *via* the experimentally measured half-cell reaction entropy (ΔS, eq 10) of $[Fe(CN)_6]^{3-}/[Fe(CN)_6]^{4-}$. Both approaches showed similar cation trends on the order of $Li^+ > Na^+ > K^+ > Rb^+ > Cs^+$.

s^{-1}),[62] and Kawiak et al. (0.02 cm s^{-1}),[61] electrochemical impedance spectroscopy studies (0.06 cm s^{-1}),[29] and the current impulse method (0.06 cm s^{-1}).[27] These rates also compare well with self-exchange reaction rates k^0_{homo} of 0.7 M s^{-1} [30] (corresponding to an equivalent heterogeneous rate $k^0_{hetero}{}'$ of 0.06 cm s^{-1} using $k^0_{homo}{}' = k^0_{homo} \times [C] \times \delta_O$,[59] where [C] is the redox concentration and δ_O is the thickness of the diffusion layer of $[Fe(CN)_6]^{3-}/[Fe(CN)_6]^{4-}$ being ~10^{-6} m from $\delta_O = 1.61 D_O^{1/3} \omega^{-1/2} \nu^{1/6}$,[59] with further details found in the Table S2, Supporting Information).

Cation-Dependent Reorganization Energy of the $[Fe(CN)_6]^{3-}/[Fe(CN)_6]^{4-}$ Redox Couple. The reorganization energy for the kinetics of the $[Fe(CN)_6]^{3-}/[Fe(CN)_6]^{4-}$ redox reaction was found to increase in the order of $Cs^+ \sim Rb^+ < K^+ < Na^+ < Li^+ \sim TBA^+$ (Figures 5a and S9), which was extracted by fitting kinetic currents (Figure 4c) measured from 2 mM equimolar $[Fe(CN)_6]^{3-}/[Fe(CN)_6]^{4-}$ with 0.6 M MCl on Au using the MHC formalism.[41−43] The reorganization energy (λ) increased from 0.23 eV for Cs^+ to 0.59 eV for Li^+, which was accompanied by the increasing reaction entropy $\left(\Delta S = \frac{dE_{1/2}}{dT}\right)$ measured by the temperature-dependent formal potential of redox reactions $\left(E_{1/2} = E_0 + \frac{RT}{zF} \ln \frac{\gamma_{Ox}[Ox]}{\gamma_{Ox}[Red]} = E_0 + \frac{RT}{zF} \ln \frac{\gamma_{Ox}}{\gamma_{Red}}\right)$ as reported previously.[24] The reaction entropy of $[Fe(CN)_6]^{3-}/[Fe(CN)_6]^{4-}$ redox was found to become more negative (from −140 to −167 J mol^{-1} K^{-1}) on the order of $Li^+ < Na^+ < K^+ < Rb^+ < Cs^+$, suggesting that cations could alter the disordering within the redox solvation structure, which could consequently lead to changes in the activity of redox molecules and in the half-cell potential (from 0.89 V_{RHE} for Li^+ to 0.92 V_{RHE} for Cs^+) (Figure S3b). Figure 5a shows that the reorganization energy of the $[Fe(CN)_6]^{3-}/[Fe(CN)_6]^{4-}$ redox process can be strongly correlated with the reaction entropy, and thus the disordering in the redox solvation structure induced by the cations, where the reorganization energy increases on increasing the ordering in the solvation shell with a lower

https://dx.doi.org/10.1021/acs.jpcc.0c10492
J. Phys. Chem. C 2021, 125, 4397−4411

reaction entropy (*e.g.*, Li^+). The difference in the reorganization energy for different cations observed experimentally could be attributed to the decrease in water molecules compensated for by an increase in the number of cations (Figure 2), facilitating the reorganization of the redox solvation shell during electron transfer.

The reorganization energy for each cation did not change with cation concentration in the range of 0.06−0.6 M (Figure S9b). However, the electronic coupling energy H_{AB} obtained by fitting MHC formalism was found to increase with cation concentration and structure-breaking properties of cations in the electrolytes (Figure S9d), which can be attributed to the cation-dependent interfacial water structure induced by cations. The values of H_{AB} in this work were found in the range of 0.01−0.1 eV (Figure S9d), which were on the same order of magnitude as that reported previously, ∼0.025 eV by the theoretical approach.[63] More importantly, fitting temperature-dependent kinetics of 2 mM equimolar $[Fe(CN)_6]^{3-}/[Fe(CN)_6]^{4-}$ with 0.6 M MCl on Au on increasing the temperature from 293 to 323 K (K^+ in Figure 5b, Li^+ in Figure 5c and Figure S10c−f) using MHC revealed that the reorganization energy is not temperature-dependent (Figure 5d). Moreover, the activation energy obtained from the temperature-dependent exchange current density of $[Fe(CN)_6]^{3-}/[Fe(CN)_6]^{4-}$ in 0.6 M MCl was found to be cation-dependent (Figure S10i−l), increasing from 0.17 eV for K^+ to 0.3 eV for Li^+ (Figure 5d), which was proportional to λ, with a fitted value of $\frac{E_a}{\lambda} = \frac{1}{2}$. This ratio is in agreement with that reported previously $\left(\frac{1}{1.5} > \frac{E_a}{\lambda} > \frac{1}{3}\right)$ for charge-transfer kinetics of lithium-ion intercalation in porous electrodes.[42] Furthermore, combining the analytical expression of exchange current density in MHC formalism and the Arrhenius equation, the theoretical value of the ratio of $\frac{E_a}{\lambda}$ is estimated to be $\sim\frac{1}{3.8}$, in agreement with experiments (Figure 5a). Both temperature-independent reorganization energy and the activation energy of the exchange current density proportional to the reorganization energy provide compelling evidence[41] for MHC electron-transfer kinetics of $[Fe(CN)_6]^{3-}/[Fe(CN)_6]^{4-}$ redox in this work.

The reorganization energy obtained from the kinetics of $[Fe(CN)_6]^{3-}/[Fe(CN)_6]^{4-}$ measured on Au (Figure 5) in this work is equal to half of those measured previously for that of the corresponding homogenous reaction kinetics (1.1 eV),[45] which is in agreement with the prediction from the Marcus theory.[59] In addition, the computed reorganization energy of 0.83 eV for the kinetics of $[Fe(CN)_6]^{3-}/[Fe(CN)_6]^{4-}$ redox at the electrode surface found by Ghosh et al.[46] using an implicit Born model, having no cations in the solvation shell of redox anions, is larger than that found in this study. Moreover, the reorganization energies extracted from the measured electron-transfer kinetics of $[Fe(CN)_6]^{3-}/[Fe(CN)_6]^{4-}$ (in 0.25 M CF_3COONa, λ = 1.13 eV)[64] and ferrocene/ferrocenium ($[Fe(C_5H_5)_2]^+/[Fe(C_5H_5)_2]^0$) (in 1 M $HClO_4$, λ = 0.85 eV) tethered on the thiol monolayer assembled on Au[43] are larger than those in this work. We propose that these differences can be attributed largely to different static dielectric constants at the electrified interface assumed and/or the distance of $[Fe(CN)_6]^{3-}/[Fe(CN)_6]^{4-}$ (20 Å) from the electrified interface than those in the electrolyte of this study (estimated as ∼12−17 Å).

In the Marcus theory,[40,59,63,65] the reorganization energy represents the energy necessary to transform the nuclear configurations in the reactant and the solvent to those of the product state. The total reorganization energy of the electron-transfer is represented by $\lambda = \lambda_i + \lambda_o$, where λ_i is the inner component of the reorganization of the chemical bond of redox species and λ_o corresponds to the outer contribution of solvent reorganization during electron-transfer processes. The inner component of the reorganization energy was estimated at 0.01 eV by the George−Griffith model (Appendix S2),[63,65] which is shown to be negligible compared to the outer reorganization energy λ_o. Following the Born solvation model of outer reorganization energy, we estimate the cation-dependent reorganization energy using the following equation[42,59]

$$\lambda \approx \lambda_o = \lambda_{SOLV} = \frac{e^2}{8\pi\varepsilon_0 k_B T}\left(\frac{1}{a_0} - \frac{1}{2d}\right)\left(\frac{1}{\varepsilon_{op}} - \frac{1}{\varepsilon_s}\right) \quad (8)$$

where ε_0 is the permittivity of free space, a_0 is the effective radius of the reactant, d is the distance from the center of $[Fe(CN)_6]^{3-}/[Fe(CN)_6]^{4-}$ to the surface of the electrode, ε_{op} is the optical dielectric constant, and ε_s is the static dielectric constant of the electrolyte near the electrified interface. However, this continuum model assumes that the ionic environment is described by structureless point particles within the Debye−Hückel theory and the static dielectric constant is independent of the electrolyte concentration. To take into account the effect of the ionic environment, Marcus[66] and Ghosh et al.[46] further suggested a reorganization energy model by

$$\lambda_{IONIC} = \frac{e^2}{8\pi\varepsilon_0 k_B T}\left[\left(\frac{1}{a_0} - \frac{1}{2d}\right)\left(\frac{1}{\varepsilon_{op}} - \frac{1}{\varepsilon_s}\right) + \frac{1}{2d\varepsilon_s}\left(\frac{2\kappa d + e^{-\kappa(2d-a)}\left(1 + \frac{(\kappa a)^2}{2}\right)}{1 + \kappa d + e^{-\kappa(2d-a)}\frac{\kappa^2 a^3}{6d}} - 1\right)\right] \quad (9)$$

where κ is the inverse Debye length, where $\kappa^{-1} = \left(\frac{\varepsilon_0\varepsilon_s k_B T}{e^2 N_A \sum_i Z_i^2 C_i}\right)^{0.5}$,[67] Z_i and C_i are the charge and concentration of species i in the electrolyte, respectively, e is the elementary charge, N_A is the Avogadro constant, ε_0 is the permittivity of free space, and ε_s is the static dielectric constant of the solvent.

Using the effective radius of the redox, which is the distance between Fe and O (RDF) (5.5 Å in Figure 2c,d), as a_0 and the distance d between the redox center and the electrode, which is the sum of the effective radius of the redox and the diameter of the cations, as $d = a_0 + d_{cation}$ (d_{Cs} = 11.6 Å and d_{Li} = 7 Å),[19] the optical dielectric constant of water was found to be 1.8[47,68] and the static dielectric constant at the electrified interface was found to be cation-dependent (Figure 5e), in the orders of Li^+ (18) > Na^+ (6.4) > K^+ (4.1) > Rb^+ (3.2) > Cs^+ (3) and Li^+ (9) > Na^+ (3) > K^+ (2) > Rb^+ (1.8) ∼ Cs^+ (1.8) using reorganization energy models without (λ_{SOLV}) and with (λ_{IONIC}) ionic environment effects, respectively, which are smaller than the dielectric constants in bulk solutions of chloride salts of Li^+, Na^+, K^+, Rb^+, and Cs (∼70), reported

https://dx.doi.org/10.1021/acs.jpcc.0c10492
J. Phys. Chem. C 2021, 125, 4397−4411

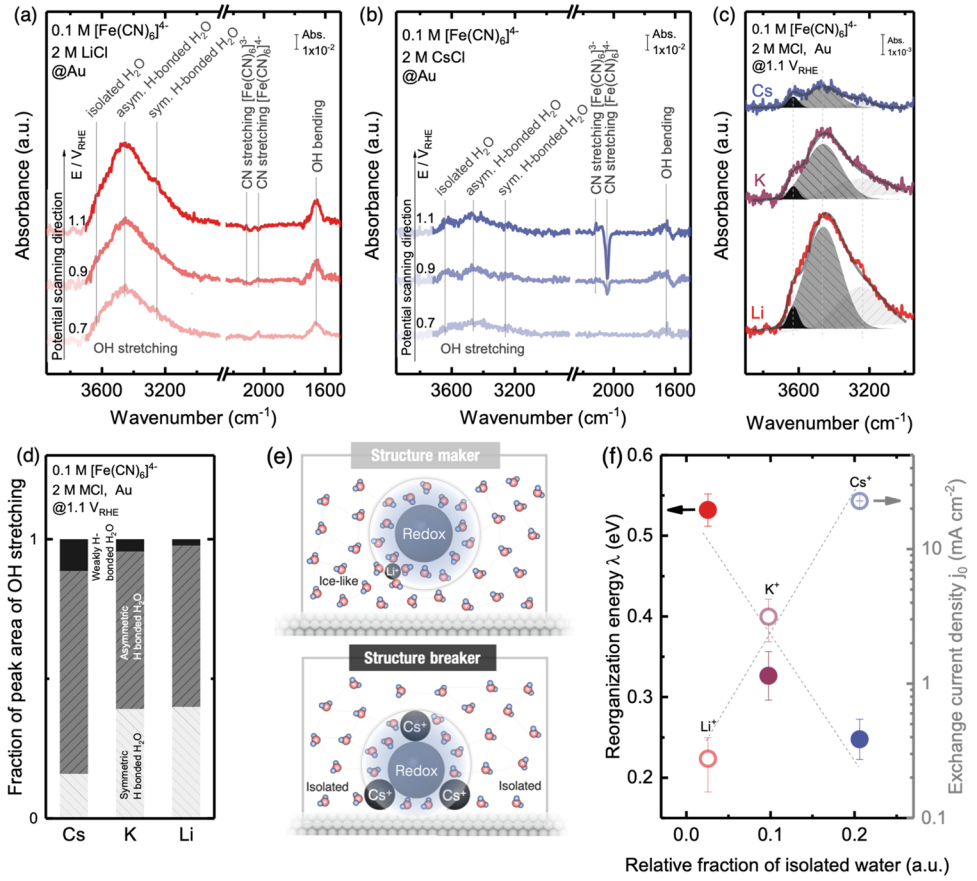

Figure 6. Altering interfacial structure at the Au surface in aqueous electrolytes through noncovalent interactions associated with the redox center, inert cations, water molecules, and Au surface. *In situ* SEIRAS spectra of oxidation of 0.1 M $[Fe(CN)_6]^{4-}$ in an aqueous solution of 2 M chloride salts of (a) Li^+ and (b) Cs^+. (c) Cation trends of OH stretching during $[Fe(CN)_6]^{4-}$ oxidation at 1.1 V_{RHE}. (d) Comparison of the relative peak area of weakly H-bonded water and asymmetric and symmetric H-bonded water. (e) Scheme summarizing the proposed mechanisms of cation-dependent kinetics where structure-breaking cations could promote weakly H-bonded water molecules at the metal surface and make the redox solvation shell disordered with loosely bonded water molecules; structure-making cations could promote a strongly hydrogen-bonded (ice-like) interfacial water layer and make the redox solvation shell ordered with tightly bonded water molecules. (f) Reorganization energy λ and exchange current density j_0 of the $[Fe(CN)_6]^{3-}/[Fe(CN)_6]^{4-}$ redox (Figures 4 and 5) as a function of the relative fraction of the weakly H-bonded water peak area in OH stretching band features.

previously.[69,70] The experimentally measured cation-dependent reorganization energy values in Figure 5a can be reproduced using this formula. Moreover, using these dielectric constants, we could predict the experimentally measured cation-dependent trend in the reaction entropy of $[Fe(CN)_6]^{3-}/[Fe(CN)_6]^{4-}$ [24] using the Born model of reaction entropy[24,71]

$$\Delta S = \frac{e^2 N_A}{8\pi\varepsilon_0\varepsilon_s T}\left(\frac{d\ln\varepsilon_s}{dT}\right)\left(\frac{Z_{ox}^2}{r_{ox}} - \frac{Z_{red}^2}{r_{red}}\right) \quad (10)$$

where T is temperature and z and r are the charge and ionic radii of redox species, respectively. Considering the temperature-dependence term, $\left(\frac{d\ln\varepsilon_s}{dT}\right) \approx -1.42$,[72] which is similar to that of pure water for approximation (identical for all cations), the interfacial static dielectric constant extracted *via* reaction entropy showed similar cation dependence (Figure 5e), on the order of Li^+ (4.2) > Na^+ (4.1) > K^+ (4.0) > Rb^+ (3.8) > Cs^+ (3.6). The difference between the Born model and experimental values is larger for other cations (Li^+, Na^+, Rb^+, and Cs^+), which might be attributed to the influence of the cation on the temperature dependence of the dielectric constant, where a larger temperature dependence of ε_s is expected for Li^+ (structure-making ions) and a smaller temperature dependence of ε_s is expected for Cs^+ (structure-breaking ions). These estimated static dielectric constants at the electrified interface are much smaller than those of bulk water (78)[70] and bulk solutions (30−75),[69,73] as seen from previous experimental[69,70] and MD simulations.[73] This result is in agreement with previous MD simulations of confined water at the planar surface,[75,76] which reveals a much reduced static dielectric constant (in the range of 1−5). Further support comes from experimental studies,[68] where the local capacitance measurements for water were confined between two atomically flat walls separated by various distances down to 1 nm, suggesting the presence of an interfacial layer with a vanishingly small polarization such that its out-of-plane dielectric constant is only ∼2, which can be attributed to the reduced rotational freedom of water dipoles near surfaces. In addition, interfacial water within spherical cavities (40−60)[76] and the spherical solute surface (4−9)[77] has been reported to have a static dielectric constant greatly different from the bulk. Moreover, cation concentrations at the electrified interface are shown to be 60 times greater than those in the bulk,[78,79] which can alter the interfacial dielectric constant. Below, we provide

https://dx.doi.org/10.1021/acs.jpcc.0c10492
J. Phys. Chem. C 2021, 125, 4397−4411

support to cation-dependent solvation environments at the electrified interface from *in situ* surface-enhanced FTIR measurements, which can potentially give rise to cation-dependent static dielectric constants at the electrified interface.

Cation-Dependent Solvation Structures at the Electrified Interface. We employed *in situ* SEIRAS to probe $[Fe(CN)_6]^{3-}/[Fe(CN)_6]^{4-}$ redox centers and solvation structures on Au as a function of voltage in the presence of 2 M MCl, including Li^+, K^+, and Cs^+, where CN stretching (~2200−2000 cm^{-1}), OH stretching (~3600−3200 cm^{-1}), and HOH bending (~1700−1600 cm^{-1}) were probed (Figures 6, S14, and S15). Figure 6a,b shows *in situ* SEIRAS spectra of $[Fe(CN)_6]^{4-}$ oxidation in the presence of Cs^+ and Li^+, respectively, and those with K^+ are shown in Figure S14a−c for comparison. The peak growth at 2116 cm^{-1} and peak reduction at ~2040 cm^{-1} were observed when the potential was increased from 0.7 to 1.1 V_{RHE} (the equilibrium potential of 2 mM $[Fe(CN)_6]^{3-}/[Fe(CN)_6]^{4-}$ in 2 M MCl is ~0.9 V_{RHE}), which could be attributed to the production of $[Fe(CN)_6]^{3-}$ and consumption of $[Fe(CN)_6]^{4}$, respectively.[80]

The reverse trend was noted when the potential was reversed, as shown in Figure S14d−f. In addition, the peak intensity changes as a function of voltage were more pronounced for $[Fe(CN)_6]^{4-}$ than $[Fe(CN)_6]^{3-}$, which can be attributed to the greater negative charge of $[Fe(CN)_6]^{4-}$ and thus the greater electrostatic attraction to positively charged Au in the voltage range.[81] Moreover, *in situ* SEIRAS spectra at 1.1 V_{RHE} revealed increasing consumption of $[Fe(CN)_6]^{4-}$ and production of $[Fe(CN)_6]^{3-}$ in the order of $Li^+ < K^+ < Cs^+$, as shown in Figure S14g, in agreement with faster kinetics on the same order (Figure 4). Furthermore, the CN stretching wavenumber of 0.1 M $[Fe(CN)_6]^{4-}$ was found to shift negatively in the order of $Cs^+ < K^+ < Li^+$ at the electrified interface (Figure S14i), similar to the results from our previous FTIR and Raman measurements in bulk electrolytes.[24]

The negative shift of the C−N stretching in the order of $Cs^+ > Rb^+ > K^+ > Na^+ > Li^+$ can be attributed to the weakening of C−N bonds due to increasing water molecules and decreasing cations in the solvation environment of negatively charged $[Fe(CN)_6]^{3-}/[Fe(CN)_6]^{4-}$ redox centers.[24] This argument is further supported by X-ray absorption spectroscopy (XAS) measurements of Fe centers.[82,83] The Fe K-edge near-edge spectrum (X-ray absorption near edge structure (XANES)) of 0.2 M $[Fe(CN)_6]^{3-}$ showed a higher white line intensity than that of $[Fe(CN)_6]^{4-}$, suggesting a lower electron density (Figure S16). More interestingly, the white line intensities of the Fe K-edge of $[Fe(CN)_6]^{3-}$ and $[Fe(CN)_6]^{4-}$ were both found to increase on the order of $TBA^+ < Li^+ \sim Na^+ < K^+ < Rb^+ < Cs^+$ (with 2 M MCl added, Figure S16b,c), suggesting reduced electron densities on Fe due to noncovalent interactions in the presence of cations, having a decreased number of water molecules and increased number of cations in the solvation shell. The pre-edge peak of the Fe K-edge (Figure S16d,e) displayed a similar peak energy for all cations, revealing that the ligand field of the $[Fe(CN)_6]^{3-}/[Fe(CN)_6]^{4-}$ complex in the presence of these cations remained unchanged.

In situ SEIRAS measurements revealed cation-dependent solvation environments for the redox of $[Fe(CN)_6]^{3-}/[Fe(CN)_6]^{4-}$ at the electrified interface from OH stretching (~3600−3200 cm^{-1}) and HOH bending (~1700−1600 cm^{-1}) features, as shown in Figures 6a−c and S17, respectively. It should be noted that the OH stretching and HOH bending features in bulk electrolytes were not sensitive to the nature of cations (Figure S18) from *ex situ* ATR/FTIR measurements. The intensity of OH stretching features was shown to decrease from Li^+, K^+ to Cs^+ (Figure 6c), indicating fewer water molecules near the electrified interface. The OH stretching features were further deconvoluted into three features: weakly H-bonded water molecules at 3630 cm^{-1},[84,85] asymmetric H-bonded water molecules at 3462 cm^{-1} (water−cation interaction, *i.e.*, water in the solvation shell of cations),[84,85] and symmetric H-bonded water molecules at 3247 cm^{-1} (water−water interaction, *i.e.*, icelike water or bulk water).[84,85] The relative fraction of weakly H-bonded water molecules at the electrified interface was found to increase from Li^+, K^+ to Cs^+, while that of strongly H-bonded (asymmetric and symmetric) water molecules decreased (Figure 6d). This observation is in agreement with more cations and few water molecules observed at the electrified interface for Cs^+ relative to Li^+, as shown in the schematic (Figure 6e), which is supported by HOH bending features. The HOH bending vibration peak (Figure S17) showed similar trends in the hydrogen-bonding network of interfacial water molecules, where the peaks at ~1610 and ~1650 cm^{-1} correspond to weakly H-bonded and strongly H-bonded water molecules, respectively.[84] In the presence of Li^+, the Au surface was largely covered by strongly (symmetric and asymmetric) H-bonded water, which increased its intensity with increasing potential. In the cases of Cs^+ and K^+, the intensity of the peak at ~1650 cm^{-1} (strongly H-bonded water) was reduced compared to Li^+; its intensity increased at higher potentials, resulting in a decreased fraction of weakly H-bonded water molecules and a negative-going peak at ~1610 cm^{-1}.

Relating Cation-Dependent Kinetics to Cation-Dependent Solvation Structures at the Electrified Interface. The increased exchange current density in the order of $Li^+ < Na^+ < K^+ < Rb^+ < Cs^+$ is coupled with the decreased reorganization energy extracted from the MHC formalism.[41] The MHC model predicts increasing exchange current density with decreasing reorganization energy.[41] Using the analytical expression of the MHC exchange current density, $j_0 = \frac{2\pi H_{AB}^2}{h\sqrt{4\pi\lambda k_B T}} \frac{\sqrt{\pi\lambda}}{2} \mathrm{erfc}\left(\frac{\lambda - \sqrt{1+\sqrt{\lambda}}}{2\sqrt{\lambda}}\right)$,[41] the reorganization energy from 0.23 eV for Cs^+ to 0.59 eV for Li^+ would translate to an increase of 44 times for the exchange current density (see the Method section for more details) considering $H_{AB} \sim 0.025$ eV[63,65] for the redox of typical transition-metal complexes, which is in reasonable agreement with experimental measurements of 113 times in Figure 4.

Cation-dependent kinetics of $[Fe(CN)_6]^{3-}/[Fe(CN)_6]^{4-}$ in terms of the exchange current density and the reorganization energy can be attributed to cation-dependent solvation structures of $[Fe(CN)_6]^{3-}/[Fe(CN)_6]^{4-}$ at the electrified interface. As similar cation-dependent kinetic current densities were found for RDE measurements collected from Pt (Figure S12) to those obtained from Au, the cation-dependent kinetics of $[Fe(CN)_6]^{3-}/[Fe(CN)_6]^{4-}$ redox are unlikely derived from the positively charged interface, where Pt is expected to have less positive charge than Au near the equilibrium potential of $[Fe(CN)_6]^{3-}/[Fe(CN)_6]^{4-}$ (~0.9 V_{RHE}) due to the higher potential of zero charge of 0.72 V_{RHE} on Pt,[86] than 0.62 V_{RHE} on Au.[81] Of significance to note is that increasing the fraction of weakly H-bonded water and decreasing the fraction of

https://dx.doi.org/10.1021/acs.jpcc.0c10492
J. Phys. Chem. C 2021, 125, 4397−4411

strongly H-bonded water near the electrified interface were found to correlate with increasing exchange current density in the order of $Li^+ < K^+ < Cs^+$ in Figure 4 and decrease with the reorganization energy of $[Fe(CN)_6]^{3-}/[Fe(CN)_6]^{4-}$ redox in the order of $Li^+ > K^+ > Cs^+$ (Figure 5), as shown in Figure 6f. Having an increasing fraction of weakly H-bonded water molecules at the electrified interface on the order from Li^+, K^+ to Cs^+ (Figure 6e) supports the fact that the electrified interface of Cs^+ can have lower static dielectric constants than that in the presence of Li^+ proposed in the previous sections. This argument is in agreement with the fact that the hydrophobic interface with weakly H-bond water is shown to have lower dielectric constants than the hydrophilic one.[74] In addition, the proposed mechanism (Figure 6e) is in agreement with those reported for increasing rate constants of self-exchange reactions of $[Os(CN)_6]^{3-}/[Os(CN)_6]^{4-}$,[26,33] $[Mo(CN)_8]^{3-}/[Mo(CN)8]^{4-}$,[26] and $[W(CN)_8]^{3-}/[W(CN)8]^{4-}$[26] from $Li^+ < Na^+ < K^+ < Rb^+ < Cs^+$, where reducing the number of coordinated water molecules from cations (Figure 1a) can promote the electron-transfer kinetics by allowing closer contact of two anions with a bridging cation.[26]

CONCLUSIONS

Classical MD simulation of the bulk electrolyte containing 0.06 M $[Fe(CN)_6]^{3-}/[Fe(CN)_6]^{4-}$ redox and 0.6 M chloride salts of TBA^+, Li^+, Na^+, K^+, Rb^+, and Cs^+ showed that the solvation shell of the $[Fe(CN)_6]^{3-}/[Fe(CN)_6]^{4-}$ redox center can be significantly altered by the spectator cations in the electrolyte, where water molecules in the solvation shell tend to be displaced by cations as the cations vary from Li^+ to Cs^+, whereas the Madelung potential energy distribution analysis showed that the overall structure/dynamics of the bulk electrolyte remains essentially intact. The contribution from the solvation structures of the redox-inactive structure-making/-breaking cations to the electron-transfer kinetics of 2 mM equimolar $[Fe(CN)_6]^{3-}/[Fe(CN)_6]^{4-}$ at polycrystalline Au and Pt electrodes was systematically probed. A cation-dependent trend for the exchange current density j_0 has been observed, where structure-breaking cations are found to interact strongly with the $[Fe(CN)_6]^{3-}/[Fe(CN)_6]^{4-}$ redox center and the electrode surface, which facilitates electron transfer by lowering the reorganization energy and increasing the electronic coupling energy. At a given concentration of supporting electrolyte, the exchange current density j_0 increased with greater structure-breaking tendency of the ions in the order of $Cs^+ > Rb^+ > K^+ > Na^+ > Li^+ \sim TBA^+$. Using the Born model of reorganization energy, the static dielectric constant of water was found to decrease from 18 for Li^+ to 3 for Cs^+, significantly lower than that of bulk water at 78. The electron density on the Fe atom in $[Fe(CN)_6]^{3-}$ and $[Fe(CN)_6]^{4-}$ was found to increase with stronger structure-breaking cations, as evidenced by the higher white line intensity. *In situ* SEIRAS measurements showed that these spectator ions might also alter the H-bonding network among interfacial water molecules and thus induce changes in CN and OH stretching features. We show that Cs^+ ions could promote weakly H-bonded water, whereas Li^+ ions could promote a H-bonded water network, which might be responsible for the altered static dielectric constant of interfacial water molecules and thus the observed cation-dependent kinetics (exchange current density and reorganization energy) and reaction entropy change of $[Fe(CN)_6]^{3-}/[Fe(CN)_6]^{4-}$ redox. The findings of this study may have broader implications for the role of structure-making/-breaking spectator ions on redox reactions in concentrated electrolytes and ionic liquids. These fundamental insights into the control of solvation environments at the electrified interface can be leveraged to tune the kinetic rates and selectivity of electrochemical reactions needed for decarbonizing chemicals and fuels.

ASSOCIATED CONTENT

Supporting Information

The Supporting Information is available free of charge at https://pubs.acs.org/doi/10.1021/acs.jpcc.0c10492.

Cyclic voltammograms; Koutecky–Levich analysis; ratio of the kinetic current density to the limiting current density; classical MD-computed interaction energy, Madelung potential energy distribution and radial distribution function; concentration- and temperature-dependent kinetic current density, XANES spectra, *in situ* SEIRA spectra, *ex situ* ATR/FTIR spectra; force field parameters of classical MD simulation; summary of heterogeneous and homogeneous rate constants and reorganization energy in the literature; Marcus energy gap formalism for the Madelung potential energy distribution (PDF)

AUTHOR INFORMATION

Corresponding Authors

Botao Huang − *Electrochemical Energy Laboratory and Research Laboratory of Electronics, Massachusetts Institute of Technology, Cambridge, Massachusetts 02139, United States*; orcid.org/0000-0001-5634-5620; Email: huang73@mit.edu

Adam P. Willard − *Department of Chemistry, Massachusetts Institute of Technology, Cambridge, Massachusetts 02139, United States*; orcid.org/0000-0002-0934-4737; Email: awillard@mit.edu

Yang Shao-Horn − *Electrochemical Energy Laboratory, Department of Mechanical Engineering, and Department of Material Science and Engineering, Massachusetts Institute of Technology, Cambridge, Massachusetts 02139, United States*; orcid.org/0000-0001-8714-2121; Email: shaohorn@mit.edu

Authors

Kyaw Hpone Myint − *Department of Chemistry, Massachusetts Institute of Technology, Cambridge, Massachusetts 02139, United States*

Yanming Wang − *Research Laboratory of Electronics, Massachusetts Institute of Technology, Cambridge, Massachusetts 02139, United States*; orcid.org/0000-0002-0912-681X

Yirui Zhang − *Electrochemical Energy Laboratory and Department of Mechanical Engineering, Massachusetts Institute of Technology, Cambridge, Massachusetts 02139, United States*

Reshma R. Rao − *Electrochemical Energy Laboratory and Research Laboratory of Electronics, Massachusetts Institute of Technology, Cambridge, Massachusetts 02139, United States*; orcid.org/0000-0002-6655-3105

Jame Sun − *Electrochemical Energy Laboratory and Department of Mechanical Engineering, Massachusetts Institute of Technology, Cambridge, Massachusetts 02139, United States*

Sokseiha Muy − *Electrochemical Energy Laboratory and Research Laboratory of Electronics, Massachusetts Institute of Technology, Cambridge, Massachusetts 02139, United States*

Yu Katayama − *Electrochemical Energy Laboratory, Massachusetts Institute of Technology, Cambridge, Massachusetts 02139, United States; Department of Applied Chemistry, Graduate School of Sciences and Technology for Innovation, Yamaguchi University, Ube 755-8611, Japan;* orcid.org/0000-0002-7842-2938

Juan Corchado Garcia − *Electrochemical Energy Laboratory and Research Laboratory of Electronics, Massachusetts Institute of Technology, Cambridge, Massachusetts 02139, United States*

Dimitrios Fraggedakis − *Electrochemical Energy Laboratory and Department of Chemistry, Massachusetts Institute of Technology, Cambridge, Massachusetts 02139, United States*

Jeffrey C. Grossman − *Department of Material Science and Engineering, Massachusetts Institute of Technology, Cambridge, Massachusetts 02139, United States;* orcid.org/0000-0003-1281-2359

Martin Z. Bazant − *Department of Mathematics and Department of Chemical Engineering, Massachusetts Institute of Technology, Cambridge, Massachusetts 02139, United States;* orcid.org/0000-0002-8200-4501

Kang Xu − *Battery Science Branch, Sensor and Electron Devices Directorate, U.S. Army Research Laboratory, Adelphi, Maryland 20783-1197, United States*

Complete contact information is available at: https://pubs.acs.org/10.1021/acs.jpcc.0c10492

Author Contributions

B.H., A.P.W., and Y.S.-H. designed the experiments. B.H. carried out electrochemical experiments. K.H.M. and Y.W. performed classical MD calculations. Y.Z. and B.H. carried out *in situ* SEIRAS experiments. B.H. and J.C.G. conducted XAS measurements. B.H. performed the analysis and prepared the initial manuscript. All authors contributed to the discussion and revision of the manuscript.

Notes

The authors declare no competing financial interest.

■ ACKNOWLEDGMENTS

This work was supported in part by the "Solid State Solar-Thermal Energy Conversion Center (S^3TEC)", an Energy Frontier Research Center funded by the U.S. Department of Energy, Office of Science, BES, under Award number DE-SC0001299/DE-FG02-09ER46577; by a grant from the Innovation and Technology Commission of the Hong Kong Special Administrative Region, China (Project no. ITS/020/16FP); and by a grant from MISTI-France, MISTI Global Seed Fund program (Project no. 3157370). Y.K. acknowledges funding from the JSPS KAKENHI under Grant number 19 K15360 and JSPS Open Partnership Joint Research Projects (JPJSBP 120209925).

■ REFERENCES

(1) Walter, M. G.; Warren, E. L.; McKone, J. R.; Boettcher, S. W.; Mi, Q.; Santori, E. A.; Lewis, N. S. Solar Water Splitting Cells. *Chem. Rev.* **2010**, *110*, 6446−6473.

(2) Weinstein, L. A.; Loomis, J.; Bhatia, B.; Bierman, D. M.; Wang, E. N.; Chen, G. Concentrating Solar Power. *Chem. Rev.* **2015**, *115*, 12797−12838.

(3) Carrillo, A. J.; González-Aguilar, J.; Romero, M.; Coronado, J. M. Solar Energy on Demand: A Review on High Temperature Thermochemical Heat Storage Systems and Materials. *Chem. Rev.* **2019**, *119*, 4777−4816.

(4) Hwang, J.; Rao, R. R.; Giordano, L.; Katayama, Y.; Yu, Y.; Shao-Horn, Y. Perovskites in Catalysis and Electrocatalysis. *Science* **2017**, *358*, 751.

(5) Suntivich, J.; Gasteiger, H. A.; Yabuuchi, N.; Nakanishi, H.; Goodenough, J. B.; Shao-Horn, Y. Design Principles for Oxygen-Reduction Activity on Perovskite Oxide Catalysts for Fuel Cells and Metal−Air Batteries. *Nat. Chem.* **2011**, *3*, 546.

(6) Suntivich, J.; May, K. J.; Gasteiger, H. A.; Goodenough, J. B.; Shao-Horn, Y. A Perovskite Oxide Optimized for Oxygen Evolution Catalysis from Molecular Orbital Principles. *Science* **2011**, *334*, 1383.

(7) Hong, W. T.; Risch, M.; Stoerzinger, K. A.; Grimaud, A.; Suntivich, J.; Shao-Horn, Y. Toward the Rational Design of Non-Precious Transition Metal Oxides for Oxygen Electrocatalysis. *Energy Environ. Sci.* **2015**, *8*, 1404−1427.

(8) Strmcnik, D.; Lopes, P. P.; Genorio, B.; Stamenkovic, V. R.; Markovic, N. M. Design Principles for Hydrogen Evolution Reaction Catalyst Materials. *Nano Energy* **2016**, *29*, 29−36.

(9) Tymoczko, J.; Calle-Vallejo, F.; Schuhmann, W.; Bandarenka, A. S. Making the Hydrogen Evolution Reaction in Polymer Electrolyte Membrane Electrolysers Even Faster. *Nat. Commun.* **2016**, *7*, No. 10990.

(10) Sheng, W.; Gasteiger, H. A.; Shao-Horn, Y. Hydrogen Oxidation and Evolution Reaction Kinetics on Platinum: Acid vs Alkaline Electrolytes. *J. Electrochem. Soc.* **2010**, *157*, B1529−B1536.

(11) Sheng, W.; Zhuang, Z.; Gao, M.; Zheng, J.; Chen, J. G.; Yan, Y. Correlating Hydrogen Oxidation and Evolution Activity on Platinum at Different PH with Measured Hydrogen Binding Energy. *Nat. Commun.* **2015**, *6*, No. 5848.

(12) Zheng, J.; Sheng, W.; Zhuang, Z.; Xu, B.; Yan, Y. Universal Dependence of Hydrogen Oxidation and Evolution Reaction Activity of Platinum-Group Metals on PH and Hydrogen Binding Energy. *Sci. Adv.* **2016**, *2*, No. e1501602.

(13) Rossmeisl, J.; Chan, K.; Skúlason, E.; Björketun, M. E.; Tripkovic, V. On the PH Dependence of Electrochemical Proton Transfer Barriers. *Catal. Today* **2016**, *262*, 36−40.

(14) Cheng, T.; Wang, L.; Merinov, B. V.; Goddard, W. A. Explanation of Dramatic PH-Dependence of Hydrogen Binding on Noble Metal Electrode: Greatly Weakened Water Adsorption at High PH. *J. Am. Chem. Soc.* **2018**, *140*, 7787−7790.

(15) Tymoczko, J.; Colic, V.; Ganassin, A.; Schuhmann, W.; Bandarenka, A. S. Influence of the Alkali Metal Cations on the Activity of Pt(1 1 1) towards Model Electrocatalytic Reactions in Acidic Sulfuric Media. *Catal. Today* **2015**, *244*, 96−102.

(16) Strmcnik, D.; Kodama, K.; van der Vliet, D.; Greeley, J.; Stamenkovic, V. R.; Marković, N. M. The Role of Non-Covalent Interactions in Electrocatalytic Fuel-Cell Reactions on Platinum. *Nat. Chem.* **2009**, *1*, 466−472.

(17) Strmcnik, D.; van der Vliet, D. F.; Chang, K.-C.; Komanicky, V.; Kodama, K.; You, H.; Stamenkovic, V. R.; Marković, N. M. Effects of Li+, K+, and Ba2+ Cations on the ORR at Model and High Surface Area Pt and Au Surfaces in Alkaline Solutions. *J. Phys. Chem. Lett.* **2011**, *2*, 2733−2736.

(18) Suntivich, J.; Perry, E. E.; Gasteiger, H. A.; Shao-Horn, Y. The Influence of the Cation on the Oxygen Reduction and Evolution Activities of Oxide Surfaces in Alkaline Electrolyte. *Electrocatalysis* **2013**, *4*, 49−55.

(19) Ringe, S.; Clark, E. L.; Resasco, J.; Walton, A.; Seger, B.; Bell, A. T.; Chan, K. Understanding Cation Effects in Electrochemical CO2 Reduction. *Energy Environ. Sci.* **2019**, *12*, 3001−3014.

(20) Resasco, J.; Chen, L. D.; Clark, E.; Tsai, C.; Hahn, C.; Jaramillo, T. F.; Chan, K.; Bell, A. T. Promoter Effects of Alkali Metal Cations on the Electrochemical Reduction of Carbon Dioxide. *J. Am. Chem. Soc.* **2017**, *139*, 11277−11287.

(21) Pérez-Gallent, E.; Marcandalli, G.; Figueiredo, M. C.; Calle-Vallejo, F.; Koper, M. T. M. Structure- and Potential-Dependent

Cation Effects on CO Reduction at Copper Single-Crystal Electrodes. *J. Am. Chem. Soc.* **2017**, *139*, 16412−16419.
(22) Marcus, Y. Effect of Ions on the Structure of Water: Structure Making and Breaking. *Chem. Rev.* **2009**, *109*, 1346−1370.
(23) Marcus, Y. Viscosity B-Coefficients, Structural Entropies and Heat Capacities, and the Effects of Ions on the Structure of Water. *J. Solution Chem.* **1994**, *23*, 831−848.
(24) Huang, B.; Muy, S.; Feng, S.; Katayama, Y.; Lu, Y.-C.; Chen, G.; Shao-Horn, Y. Non-Covalent Interactions in Electrochemical Reactions and Implications in Clean Energy Applications. *Phys. Chem. Chem. Phys.* **2018**, *20*, 15680−15686.
(25) Duan, J.; Feng, G.; Yu, B.; Li, J.; Chen, M.; Yang, P.; Feng, J.; Liu, K.; Zhou, J. Aqueous Thermogalvanic Cells with a High Seebeck Coefficient for Low-Grade Heat Harvest. *Nat. Commun.* **2018**, *9*, No. 5146.
(26) Metelski, P. D.; Swaddle, T. W. Cation Catalysis of Anion−Anion Electron Transfer in Aqueous Solution: Self-Exchange Reaction Kinetics of Some Hexa- and Octacyanometalate Couples at Variable Pressure. *Inorg. Chem.* **1999**, *38*, 301−307.
(27) Peter, L. M.; Dürr, W.; Bindra, P.; Gerischer, H. The Influence of Alkali Metal Cations on the Rate of the Fe(CN)64−/Fe(CN)63− Electrode Process. *J. Electroanal. Chem. Interfacial Electrochem.* **1976**, *71*, 31−50.
(28) Kůta, J.; Yeager, E. The Influence of Cations on the Electrode Kinetics of Ferricyanide-Ferrocyanide System on the Rotating Gold Electrode. *J. Electroanal. Chem. Interfacial Electrochem.* **1975**, *59*, 110−112.
(29) Campbell, S. A.; Peter, L. M. The Effect of [K+] on the Heterogeneous Rate Constant for the [Fe(CN)6]3−/[Fe(CN)6]4− Redox Couple Investigated by a.c. Impedance Spectroscope. *J. Electroanal. Chem.* **1994**, *364*, 257−260.
(30) Zahl, A.; van Eldik, R.; Swaddle, T. W. Cation-Independent Electron Transfer between Ferricyanide and Ferrocyanide Ions in Aqueous Solution. *Inorg. Chem.* **2002**, *41*, 757−764.
(31) Kurland, R. J.; Winkler, M. E. Ferrocynanide Carbon-13 NMR Line Broadening as a Probe of Electron Transfer Reactions. *J. Biochem. Biophys. Methods* **1981**, *4*, 215−225.
(32) Campion, R. J.; Deck, C. F.; King, P.; Wahl, A. C. Kinetics of Electron Exchange between Hexacyanoferrate (II) and (III) Ions. *Inorg. Chem.* **1967**, *6*, 672−681.
(33) Macartney, D. H. Kinetics of the Electron-Exchange Reaction of the Hexacyanoosmate(II/III) Couple in Aqueous Media. *Inorg. Chem.* **1991**, *30*, 3337−3342.
(34) Yamamura, T.; Watanabe, N.; Yano, T.; Shiokawa, Y. Electron-Transfer Kinetics of Np3 + /Np4 +, NpO2 +/NpO2 2 +, V2 + /V3 +, and VO2 + /VO2 + at Carbon Electrodes. *J. Electrochem. Soc.* **2005**, *152*, A830−A836.
(35) Smalley, J. F.; Finklea, H. O.; Chidsey, C. E. D.; Linford, M. R.; Creager, S. E.; Ferraris, J. P.; Chalfant, K.; Zawodzinsk, T.; Feldberg, S. W.; Newton, M. D. Heterogeneous Electron-Transfer Kinetics for Ruthenium and Ferrocene Redox Moieties through Alkanethiol Monolayers on Gold. *J. Am. Chem. Soc.* **2003**, *125*, 2004−2013.
(36) Smalley, J. F.; Feldberg, S. W.; Chidsey, C. E. D.; Linford, M. R.; Newton, M. D.; Liu, Y.-P. The Kinetics of Electron Transfer Through Ferrocene-Terminated Alkanethiol Monolayers on Gold. *J. Phys. Chem. A* **1995**, *99*, 13141−13149.
(37) Creager, S.; Yu, C. J.; Bamdad, C.; O'Connor, S.; MacLean, T.; Lam, E.; Chong, Y.; Olsen, G. T.; Luo, J.; Gozin, M.; Kayyem, J. F. Electron Transfer at Electrodes through Conjugated "Molecular Wire" Bridges. *J. Am. Chem. Soc.* **1999**, *121*, 1059−1064.
(38) Bangle, R. E.; Schneider, J.; Piechota, E. J.; Troian-Gautier, L.; Meyer, G. J. Electron Transfer Reorganization Energies in the Electrode−Electrolyte Double Layer. *J. Am. Chem. Soc.* **2020**, *142*, 674−679.
(39) Marcus, R. A. On the Theory of Oxidation-Reduction Reactions Involving Electron Transfer. I. *J. Chem. Phys.* **1956**, *24*, 966.
(40) Marcus, R. A.; Sutin, N. Electron Transfers in Chemistry and Biology. *Biochim. Biophys. Acta, Rev. Bioenerg.* **1985**, *811*, 265−322.
(41) Zeng, Y.; Smith, R. B.; Bai, P.; Bazant, M. Z. Simple Formula for Marcus−Hush−Chidsey Kinetics. *J. Electroanal. Chem.* **2014**, *735*, 77−83.
(42) Bai, P.; Bazant, M. Z. Charge Transfer Kinetics at the Solid−Solid Interface in Porous Electrodes. *Nat. Commun.* **2014**, *5*, No. 3585.
(43) Chidsey, C. E. D. Free Energy and Temperature Dependence of Electron Transfer at the Metal-Electrolyte Interface. *Science* **1991**, *251*, 919.
(44) Hartnig, C.; Koper, M. T. M. Solvent Reorganization in Electron and Ion Transfer Reactions near a Smooth Electrified Surface: A Molecular Dynamics Study. *J. Am. Chem. Soc.* **2003**, *125*, 9840−9845.
(45) Royea, W. J.; Hamann, T. W.; Brunschwig, B. S.; Lewis, N. S. A Comparison between Interfacial Electron-Transfer Rate Constants at Metallic and Graphite Electrodes. *J. Phys. Chem. B* **2006**, *110*, 19433−19442.
(46) Ghosh, S.; Soudackov, A. V.; Hammes-Schiffer, S. Electrochemical Electron Transfer and Proton-Coupled Electron Transfer: Effects of Double Layer and Ionic Environment on Solvent Reorganization Energies. *J. Chem. Theory Comput.* **2016**, *12*, 2917−2925.
(47) Liu, Y.-P.; Newton, M. D. Reorganization Energy for Electron Transfer at Film-Modified Electrode Surfaces: A Dielectric Continuum Model. *J. Phys. Chem. B* **1994**, *98*, 7162−7169.
(48) Limaye, A. M.; Ding, W.; Willard, A. P. Understanding Attenuated Solvent Reorganization Energies near Electrode Interfaces. *J. Chem. Phys.* **2020**, *152*, No. 114706.
(49) Berendsen, H. J. C.; Grigera, J. R.; Straatsma, T. P. The Missing Term in Effective Pair Potentials. *J. Phys. Chem. C* **1987**, *91*, 6269−6271.
(50) Mao, A. H.; Pappu, R. V. Crystal Lattice Properties Fully Determine Short-Range Interaction Parameters for Alkali and Halide Ions. *J. Chem. Phys.* **2012**, *137*, No. 064104.
(51) Kann, Z. R.; Skinner, J. L. A Scaled-Ionic-Charge Simulation Model That Reproduces Enhanced and Suppressed Water Diffusion in Aqueous Salt Solutions. *J. Chem. Phys.* **2014**, *141*, No. 104507.
(52) Leontyev, I.; Stuchebrukhov, A. Accounting for Electronic Polarization in Non-Polarizable Force Fields. *Phys. Chem. Chem. Phys.* **2011**, *13*, 2613−2626.
(53) Leontyev, I. V.; Stuchebrukhov, A. A. Electronic Continuum Model for Molecular Dynamics Simulations. *J. Chem. Phys.* **2009**, *130*, No. 085102.
(54) Limaye, A. M.; Willard, A. P. Modeling Interfacial Electron Transfer in the Double. *J. Phys. Chem. C* **2020**, *124*, 1352−1361.
(55) Sun, H. Force Field for Computation of Conformational Energies, Structures, and Vibrational Frequencies of Aromatic Polyesters. *J. Comput. Phys.* **1994**, *15*, 752−768.
(56) *MedeA-2.22*; Materials Design, Inc.: San Diego, CA, 2018.
(57) Prampolini, G.; Yu, P.; Pizzanelli, S.; Cacelli, I.; Yang, F.; Zhao, J.; Wang, J. Structure and Dynamics of Ferrocyanide and Ferricyanide Anions in Water and Heavy Water: An Insight by MD Simulations and 2D IR Spectroscopy. *J. Phys. Chem. B* **2014**, *118*, 14899−14912.
(58) Ryckaert, J.-P.; Ciccotti, G.; Berendsen, H. J. C. Numerical Integration of the Cartesian Equations of Motion of a System with Constraints: Molecular Dynamics of n-Alkanes. *J. Comput. Phys.* **1977**, *23*, 327−341.
(59) Bard, A. J.; Faulkner, L. R. *Electrochemical Methods: Fundamentals and Applications*, 2nd ed.; John Wiley & Sons, Inc.: New York, 2000.
(60) Katayama, Y.; Nattino, F.; Giordano, L.; Hwang, J.; Rao, R. R.; Andreussi, O.; Marzari, N.; Shao-Horn, Y. An In Situ Surface-Enhanced Infrared Absorption Spectroscopy Study of Electrochemical CO2 Reduction: Selectivity Dependence on Surface C-Bound and O-Bound Reaction Intermediates. *J. Phys. Chem. C* **2019**, *123*, 5951−5963.
(61) Kawiak, J.; Jędral, T.; Galus, Z. A Reconsideration of the Kinetic Data for the Fe(CN)63−/Fe(CN)64− System. *J. Electroanal. Chem. Interfacial Electrochem.* **1983**, *145*, 163−171.

https://dx.doi.org/10.1021/acs.jpcc.0c10492
J. Phys. Chem. C 2021, 125, 4397−4411

(62) Angell, D. H.; Dickinson, T. The Kinetics of the Ferrous/Ferric and Ferro/Ferricyanide Reactions at Platinum and Gold Electrodes: Part I. Kinetics at Bare-Metal Surfaces. *J. Electroanal. Chem. Interfacial Electrochem.* **1972**, *35*, 55−72.
(63) Bolton, J. R.; Archer, M. D. Basic Electron-Transfer Theory. *Electron Transfer in Inorganic, Organic, and Biological Systems*; Advances in Chemistry; American Chemical Society, 1991; Vol. *228*, pp 7−23.
(64) Terrettaz, S.; Becka, A. M.; Traub, M. J.; Fettinger, J. C.; Miller, C. J. Omega.-Hydroxythiol Monolayers at Au Electrodes. 5. Insulated Electrode Voltammetric Studies of Cyano/Bipyridyl Iron Complexes. *J. Phys. Chem. D* **1995**, *99*, 11216−11224.
(65) Newton, M. D.; Sutin, N. Electron Transfer Reactions in Condensed Phases. *Annu. Rev. Phys. Chem.* **1984**, *35*, 437−480.
(66) Marcus, R. A. On the Theory of Electron-Transfer Reactions. VI. Unified Treatment for Homogeneous and Electrode Reactions. *J. Chem. Phys.* **1965**, *43*, 679−701.
(67) Kohonen, M. M.; Karaman, M. E.; Pashley, R. M. Debye Length in Multivalent Electrolyte Solutions. *Langmuir* **2000**, *16*, 5749−5753.
(68) Fumagalli, L.; Esfandiar, A.; Fabregas, R.; Hu, S.; Ares, P.; Janardanan, A.; Yang, Q.; Radha, B.; Taniguchi, T.; Watanabe, K.; Gomila, G.; Novoselov, K. S.; Geim, A. K. Anomalously Low Dielectric Constant of Confined Water. *Science* **2018**, *360*, 1339.
(69) Nörtemann, K.; Hilland, J.; Kaatze, U. Dielectric Properties of Aqueous NaCl Solutions at Microwave Frequencies. *J. Phys. Chem. A* **1997**, *101*, 6864−6869.
(70) Haggis, G. H.; Hasted, J. B.; Buchanan, T. J. The Dielectric Properties of Water in Solutions. *J. Chem. Phys.* **1952**, *20*, 1452−1465.
(71) Hupp, J. T.; Weaver, M. J. Solvent, Ligand, and Ionic Charge Effects on Reaction Entropies for Simple Transition-Metal Redox Couples. *Inorg. Chem.* **1984**, *23*, 3639−3644.
(72) Owen, B. B.; Miller, R. C.; Milner, C. E.; Cogan, H. L. The Dielectric Constant of Water as a Function of Temperature and Pressure[1,2]. *J. Phys. Chem. S* **1961**, *65*, 2065−2070.
(73) Chandra, A. Static Dielectric Constant of Aqueous Electrolyte Solutions: Is There Any Dynamic Contribution? *J. Chem. Phys.* **2000**, *113*, 903−905.
(74) Varghese, S.; Kannam, S. K.; Hansen, J. S.; Sathian, S. P. Effect of Hydrogen Bonds on the Dielectric Properties of Interfacial Water. *Langmuir* **2019**, *35*, 8159−8166.
(75) Bonthuis, D. J.; Gekle, S.; Netz, R. R. Dielectric Profile of Interfacial Water and Its Effect on Double-Layer Capacitance. *Phys. Rev. Lett.* **2011**, *107*, No. 166102.
(76) Senapati, S.; Chandra, A. Dielectric Constant of Water Confined in a Nanocavity. *J. Phys. Chem. B* **2001**, *105*, 5106−5109.
(77) Dinpajooh, M.; Matyushov, D. V. Dielectric Constant of Water in the Interface. *J. Chem. Phys.* **2016**, *145*, No. 014504.
(78) Garlyyev, B.; Xue, S.; Watzele, S.; Scieszka, D.; Bandarenka, A. S. Influence of the Nature of the Alkali Metal Cations on the Electrical Double-Layer Capacitance of Model Pt(111) and Au(111) Electrodes. *J. Phys. Chem. Lett.* **2018**, *9*, 1927−1930.
(79) Xue, S.; Garlyyev, B.; Auer, A.; Kunze-Liebhäuser, J.; Bandarenka, A. S. How the Nature of the Alkali Metal Cations Influences the Double-Layer Capacitance of Cu, Au, and Pt Single-Crystal Electrodes. *J. Phys. Chem. C* **2020**, *124*, 12442−12447.
(80) Kamoshida, N.; Kasahara, S.; Ikemiya, N.; Hoshi, N.; Nakamura, M.; Einaga, Y. In Situ ATR-IR Study of Fe(CN)63−/Fe(CN)64− Redox System on Boron-Doped Diamond Electrode. *Diamond Relat. Mater.* **2019**, *93*, 50−53.
(81) Bodé, D. D.; Andersen, T. N.; Eyring, H. Cation Effects on the Potentials of Zero Charge of Gold, Silver, and Mercury Electrodes. *J. Electrochem. Soc.* **1967**, *114*, 72−75.
(82) Ross, M.; Andersen, A.; Fox, Z. W.; Zhang, Y.; Hong, K.; Lee, J.-H.; Cordones, A.; March, A. M.; Doumy, G.; Southworth, S. H.; Marcus, M. A.; Schoenlein, R. W.; Mukamel, S.; Govind, N.; Khalil, M. Comprehensive Experimental and Computational Spectroscopic Study of Hexacyanoferrate Complexes in Water: From Infrared to X-Ray Wavelengths. *J. Phys. Chem. B* **2018**, *122*, 5075−5086.
(83) Penfold, T. J.; Reinhard, M.; Rittmann-Frank, M. H.; Tavernelli, I.; Rothlisberger, U.; Milne, C. J.; Glatzel, P.; Chergui, M. X-Ray Spectroscopic Study of Solvent Effects on the Ferrous and Ferric Hexacyanide Anions. *J. Phys. Chem. A* **2014**, *118*, 9411−9418.
(84) Ataka, K.; Yotsuyanagi, T.; Osawa, M. Potential-Dependent Reorientation of Water Molecules at an Electrode/Electrolyte Interface Studied by Surface-Enhanced Infrared Absorption Spectroscopy. *J. Phys. Chem. R* **1996**, *100*, 10664−10672.
(85) Yamakata, A.; Osawa, M. Destruction of the Water Layer on a Hydrophobic Surface Induced by the Forced Approach of Hydrophilic and Hydrophobic Cations. *J. Phys. Chem. Lett.* **2010**, *1*, 1487−1491.
(86) Rizo, R.; Sitta, E.; Herrero, E.; Climent, V.; Feliu, J. M. Towards the Understanding of the Interfacial PH Scale at Pt(111) Electrodes. *Electrochim. Acta* **2015**, *162*, 138−145.
(87) Kawiak, J.; Kulesza, P. J.; Galus, Z. A Search for Conditions Permitting Model Behavior of the Fe(CN)3−/4−6 System. *J. Electroanal. Chem. Interfacial Electrochem.* **1987**, *226*, 305−314.
(88) Risch, M.; Stoerzinger, K. A.; Regier, T. Z.; Peak, D.; Sayed, S. Y.; Shao-Horn, Y. Reversibility of Ferri-/Ferrocyanide Redox during Operando Soft X-Ray Spectroscopy. *J. Phys. Chem. C* **2015**, *119*, 18903−18910.

https://dx.doi.org/10.1021/acs.jpcc.0c10492
J. Phys. Chem. C 2021, 125, 4397−4411